Documentation - CTE2016

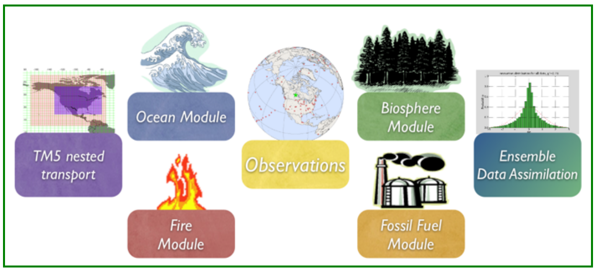

To learn more about a CarbonTracker component, click on one of the above images.
Or **download the full PDF version** for convenience.

TM5 Nested Transport [go to top]

1. Introduction

The link between observations of CO_2 in the atmosphere and the exchange of CO_2 at the Earth's surface is transport in the atmosphere: storm systems, cloud complexes, and weather of all sorts cause winds that transport CO_2 around the world. As a result, local events like fires, forest growth, and ocean upwelling can have impacts at remote locations. To simulate the winds and the weather, CarbonTracker uses sophisticated numerical models that are driven by the daily weather forecasts from the specialized meteorological centers of the world. Since CO_2 does not decay or react in the lower atmosphere, the influence of emissions and uptake in locations such as North America and Europe are ultimately seen in our measurements even at the South Pole! Getting the transport of CO_2 just right is an enormous challenge, and costs us almost 90% of the computer resources for CarbonTracker. To represent the atmospheric transport, we use the Transport Model 5 (**TM5**). This is a community-supported model whose development is shared among many scientific groups with different areas of expertise. TM5 is used for many applications other than CarbonTracker, including forecasting air-quality, studying the dispersion of aerosols in the tropics, tracking biomass burning plumes, and predicting pollution levels that future generations might have to deal with.

2. Detailed Description

TM5 is a global model with two-way nested grids; regions for which high-resolution simulations are desired can be nested in a coarser grid spanning the global domain. The advantage to this approach is that transport simulations can be performed with a regional focus without the need for boundary conditions from other models. Further, this approach allows measurements outside the "zoom" domain to constrain regional fluxes in the data assimilation, and ensures that regional estimates are consistent with global constraints. TM5 is based on the predecessor model TM3, with improvements in the advection scheme, vertical diffusion parameterization, and meteorological preprocessing of the wind fields (Krol et al., 2005). The model is developed and maintained jointly by the **Institute for Marine and Atmospheric Research Utrecht (IMAU, The Netherlands)**, the **Joint Research Centre (JRC, Italy)**, the **Royal Netherlands Meteorological Institute (KNMI, The Netherlands)**, and **NOAA ESRL (USA)**. In CarbonTracker, TM5 separately simulates advection, convection (deep and shallow), and vertical diffusion in the planetary boundary layer and free troposphere.

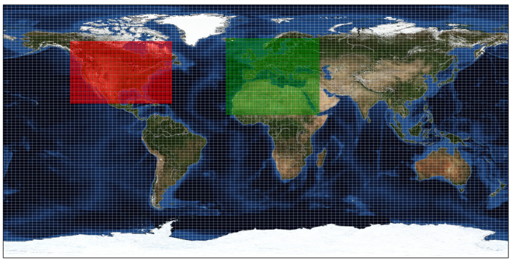

The winds which drive TM5 come from the **European Center for Medium range Weather Forecast (ECMWF)** operational forecast model. This "parent" model currently runs with ~25 km horizontal resolution and 25 layers in the vertical. The carbon dioxide levels predicted by CarbonTracker do not feed back onto these predictions of winds. In contrast to earlier verions of CarbonTracker, we currently use the convection fields directly from ECMWF (whereas before they were calculated using the Tiedtke convection scheme).

For use in TM5, the ECMWF meteorological data are preprocessed into coarser grids. In CarbonTracker Europe, TM5 is run at a global 3x2 degrees resolution with nested regions over Europe (1x1 degrees) and North America (1x1 degree). The grid over Europe is shown in the figure. TM5 runs at an external time step of three hours, but due to the symmetrical operator splitting and the refined resolution in nested grids, processes at the finest scale are repeated every 10 minutes. The vertical resolution of TM5 in CarbonTracker Europe is 25 hybrid sigma-pressure levels, unevenly spaced with more levels near the surface. Approximate heights of the mid-levels (in meters, with a surface pressure of 1012 hPa) are:

Level	Height (m)	Level	Height (m)
1	34.5	14	9076.6
2	111.9	15	10533.3
3	256.9	16	12108.3
4	490.4	17	13874.2
5	826.4	18	15860.1
6	1274.1	19	18093.2
7	1839.0	20	20590.0
8	2524.0	21	24247.3
9	3329.9	22	29859.6
10	4255.6	23	35695.0
11	5298.5	24	42551.5
12	6453.8	25	80000.0
13	7715.4		

3. Further Reading

- **The TM5 model homepage**
- **ECMWF forecast model technical documentation**
- **Peters et al., 2004, JGR paper on transport in TM5**
- **Krol et al., 2005, ACP overview paper of the TM5 model**

Oceans Module [go to top]

1. Introduction

The oceans play an important role in the Earth's carbon cycle. They are the largest long-term sink for carbon and have an enormous capacity to store and redistribute CO_2 within the system. Oceanographers estimate that about 48% of the CO_2 from fossil fuel burning has been absorbed by the ocean [Sabine et al., 2004]. The dissolution of CO_2 in seawater shifts the balance of the ocean carbonate equilibrium towards a more acidic state (i.e., with a lower pH). This effect is already measurable [Caldeira and Wickett, 2003], and is expected to become an acute challenge to shell-forming organisms over the coming decades and centuries. Although the oceans as a whole have been a relatively steady net carbon sink, CO_2 can also come out of the oceans depending on local temperatures, biological activity, wind speeds, and ocean circulation. These processes are all considered in CarbonTracker, since they can have significant effects on the ocean sink. Improved estimates of the air-sea exchange of carbon in turn help us to understand variability of both the atmospheric burden of CO_2 and terrestrial carbon exchange.

2. Detailed Description

Oceanic uptake of CO_2 in CarbonTracker is computed using air-sea differences in partial pressure of CO_2 inferred from ocean inversions, combined with a gas transfer velocity computed from wind speeds in the atmospheric transport model.

The long-term mean air-sea fluxes, and the uncertainties associated with them, derive from the ocean interior inversions reported in Jacobson et al. [2007]. These ocean inversion flux (OIF) estimates are composed of separate preindustrial (natural) and anthropogenic flux inversions based on the methods described in Gloor et al. [2003] and biogeochemical interpretations of Gruber, Sarmiento, and Stocker [1996]. The uptake of anthropogenic CO_2 by the ocean is assumed to increase in proportion to atmospheric CO_2 levels, consistent with estimates from ocean carbon models.

For CarbonTracker Europe, contemporary pCO_2 fields were computed by summing the preindustrial and anthropogenic flux components from inversions using five different configurations of the Princeton/GFDL

MOM3 ocean general circulation model [Pacanowski and Gnanadesikan, 1998], then dividing by a gas transfer velocity computed from the European Centre for Medium-Range Weather Forecasts (ECMWF) ERA40 reanalysis. There are two small differences in first-guess fluxes in this computation from those reported in Jacobson et al. [2007]. First, the five OIF estimates all used Takahashi et al. [2002] pCO_2 estimates to provide high-resolution patterning of flux within inversion regions (the alternative "forward" model patterns were not used). To good approximation, this choice only affects the spatial and temporal distribution of flux within each of the **30 ocean inversion regions**, not the magnitude of the estimated flux. Second, wind speed differences between the ERA40 product used in the offline analysis and the ECMWF operational model used in the online CarbonTracker analysis result in small deviations from the OIF estimates.

Gas transfer velocity in CarbonTracker is parameterized as a quadratic function of wind speed following Wanninkhof [1992], using the formulation for instantaneous winds. Gas exchange is computed every 3 hours using wind speeds from the ECMWF operational model as represented by the **TM5 atmospheric transport model**. Other than the smooth trend in anthropogenic flux assumed by the OIF results, interannual variability (IAV) in the first guess ocean flux comes entirely from wind speed effects on the gas transfer velocity. This is because the ocean inversions retrieve only a long-term mean and smooth trend.

The initial release of CarbonTracker (2007A) used climatogical estimates of CO_2 partial pressure in surface waters from Takahashi et al. [2002] to compute a first-guess air-sea flux. This air-sea pCO_2 disequilibrium was modulated by a surface barometric pressure correction before being multiplied by a gas-transfer coefficient to yield a flux. Starting with CarbonTracker 2007B and in this CarbonTracker Europe release, the air-sea pCO_2 disequilibrium is imposed from analysis of the OIF results, with short-term flux variability derived from the atmospheric model wind speeds via the gas transfer coefficient. The barometric pressure correction has been removed so that climatological high- and low-pressure cells do not bias the long-term means of the first guess fluxes. In either method, the first-guess fluxes have no interannual variability (IAV) due to pCO_2 changes, such as those that occur in the tropical eastern Pacific during an El Niño. In CarbonTracker, this flux IAV must be inferred from atmospheric CO_2 signals.

Air-sea transfer is inhibited by the presence of sea ice, and for this work fluxes are scaled by the daily sea ice fraction in each gridbox provided by the ECMWF forecast data.

The first-guess fluxes described here are subject to scaling during the CarbonTracker optimization process, in which atmospheric CO_2 mole fraction observations are combined with transport simulated by the atmospheric model to infer flux signals. In this process, signals of terrestrial flux in atmospheric CO_2 distribution can be erroneously interpreted as being caused by oceanic fluxes. This flux "aliasing" or "leakage" is evident in some regions as a change in the shape of the seasonal cycle of air-sea flux. Differences between CarbonTracker posterior air-sea fluxes and those of the OIF prior fluxes are minor, but do constitute an issue that we will be investigating in the future.

3. **Further Reading**

- **NOAA Pacific Marine Environmental Laboratory (PMEL)**
- **Ocean Acidification**
- Caldeira, K., and M. E. Wickett (2003), Anthropogenic carbon and ocean pH, Nature, 425365-365.
- Gloor, M., N. Gruber, J. Sarmiento, C. L. Sabine, R. A. Feely, and C. Rödenbeck (2003), A first estimate of present and preindustrial air-sea CO_2 flux patterns based on ocean interior carbon measurements and models, Geophysical Research Letters, 30, , 10.1029/2002GL015594.
- Gruber, N., J. L. Sarmiento, and T. F. Stocker (1996), An improved method for detecting anthropogenic CO_2 in the oceans, Global Biogeochemical Cycles, 10, , 809-837.
- Jacobson, A. R., N. Gruber, J. L. Sarmiento, M. Gloor, and S. E. Mikaloff Fletcher (2007), A joint atmosphere-ocean inversion for surface fluxes of carbon dioxide: I. Methods and global-scale fluxes, Global Biogeochemical Cycles, 21, doi:10.1029/2005GB002556.
- Pacanowski, R. C., and A. Gnanadesikan (1998), Transient response in a z-level ocean model that resolves topography with partial cells, Monthly Weather Review, 126, 3248--3270.
- Sabine, C. L., R. A. Feely, N. Gruber, R. M. Key, K. Lee, J. L. Bullister, R. Wanninkhof, C. S. Wong, D. W. R. Wallace, B. Tilbrook, F. J. Millero, T. H. Peng, A. Kozyr, T. Ono, and A. F. Rios (2004), The oceanic sink for anthropogenic CO_2, Science, 305, 367-371.
- Takahashi, T., S. C. Sutherland, C. Sweeney, A. P. N. Metzl, B. Tilbrook, N. Bates, R. Wanninkhof, R. A. Feely, C. Sabine, J. Olafsson, and Y. Nojiri (2002), Global air-sea CO_2 flux based on climatological surface ocean pCO_2, and seasonal biological and temperature effects, Deep-Sea Research II, 49, , 1601--1622.
- Wanninkhof, R. (1992), Relationship between wind speed and gas exchange over the ocean, Journal of Geophysical Research, 97, 7373--7382.

Fire Module [go to top]

1. **Introduction**

Vegetation fires are an important part of the carbon cycle and have been so for many millennia. Even before human civilization began to use fires to clear land for agricultural purposes, most ecosystems were subject to natural wildfires that would rejuvenate old forests and bring important minerals to the soils. When fires consume part of the landscape in either controlled or natural burning, carbon dioxide (amongst many other gases and aerosols) is released in large quantities. Each year, vegetation fires emit more than 2 PgC as CO_2 into the atmosphere, mostly in the tropics. Currently, a large fraction of these fires is started by humans, and mostly intentionally to clear land for agriculture, or to re-fertilize soils before a new growing season. This important component of the carbon cycle is monitored mostly from space, while sophisticated 'biomass burning' models are used to estimate the amount of CO_2 emitted by each fire. Such estimates are then used in CarbonTracker to prescribe the emissions, without further refinement by our measurements.

2. **Detailed Description**

The fire module currently used in CarbonTracker is based on the Global Fire Emissions Database version 4 (GFEDv4/MCD64A1), which is used in the SiBCASA biosphere model as described **here**. The GFED4/MCD64A1 dataset consists of 0.25x0.25 degree gridded monthly burned area for the time period spanning January 1997 - December 2017. The CO_2 emissions are calculated in SiBCASA using the Burned Area and the vegetation types. The GFEDv4 burned area is based on MODIS satellite observations of fire counts. The full data set was produced by combining 500 m MODIS burned area maps with active fire data from the Tropical Rainfall Measuring Mission (TRMM) Visible and Infrared Scanner (VIRS) and the Along-Track Scanning Radiometer (ATSR) family of sensors.

Once burned area has been estimated globally, emissions of trace gases are calculated using the SiBCASA biosphere model. The seasonally changing vegetation and soil biomass stocks in the SiBCASA model are combusted based on the burned area estimate, and converted to atmospheric trace gases using estimates of fuel loads, combustion completeness, and burning efficiency.

GFED products were successfully used in recent studies of CH_4, CO_2, CO, and other trace gases.

3. **Further Reading**

- **Giglio, L. *et al.* (2013)**, Analysis of daily, monthly, and annual burned area using the fourth-generation global fire emissions database (GFED4), *J. Geophys. Res.: Biogeosciences*, 118, 317-328
- **van der Werf, G. R. *et al.* (2006)**, Interannual variability in global biomass burning emissions from 1997 to 2004, *Atm. Chem. Phys.*, 6(11), 3423-3441
- **van der Velde, I. R. *et al.* (2013)**, Biosphere model simulations of interannual variability in terrestrial $^{13}C/^{12}C$ exchange, *Global Biogeochemical Cycles*, 27(3), 637-649.
- **van der Velde, I. R. *et al.* (2014)**, Terrestrial cycling of $^{13}CO_2$ by photosynthesis, respiration, and biomass burning in SiBCASA , *Biogeosciences*, 11, 6553-6571.
- **Giglio *et al.* (2006)**, Global estimation of burned area using MODIS active fire observations, Atmos. Chem. Phys., 6, 957-974

Biosphere Module [go to top]

1. **Introduction**

The biospheric component of the carbon cycle consists of all the carbon stored in 'biomass' around us. This includes trees, shrubs, grasses, carbon within soils, dead wood, and leaf litter. Such reservoirs of carbon can exchange CO_2 with the atmosphere. Exchange starts when plants take up CO_2 during their growing season through the process called photosynthesis (uptake). Most of this carbon is released back to the atmosphere throughout the year through a process called respiration (release). This includes both the decay of dead wood and litter and the metabolic respiration of living plants. Of course, plants can also return carbon to the atmosphere when they burn, **as described here**. Even though the yearly sum of uptake and release of carbon amounts to a relatively small number (a few petagrams (one $Pg=10^{15}$ g)) of carbon per year, the flow of carbon each way is as large as 120 Pg each year. This is why the net result of these flows needs to be monitored in a system such as ours. It is also the reason we need a good physical description (model) of these flows of carbon. After all, from the atmospheric measurements we can only see the small net sum of the large two-way streams (gross fluxes). Information on what the biospheric fluxes are doing in each season, and in every location on Earth is derived from a specialized biosphere model, and fed into our system as a first guess, to be refined by our assimilation procedure.

2. **Detailed Description**

The biosphere model currently used in CarbonTracker is the Simple-Biosphere-Model-Carnegie-Ames Stanford Approach (SiBCASA) biogeochemical model. This model calculates global carbon fluxes using input from weather models to drive biophysical processes, as well as satellite observed Normalized Difference Vegetation Index (NDVI) to track plant phenology. The version of SiBCASA model output used so far was driven by year specific weather and satellite observations, and including the effects of fires on photosynthesis and respiration (see van der Velde et al., [2014], van der Werf et al., [2006] and Giglio et al., [2006]). This simulation gives 1x1 degree global fluxes on a 10-minute time resolution, which we average to monthly means for further processing.

3-Hourly Net Ecosystem Exchange (NEE) is derived directly from Gross Primary Production (GPP) and ecosystem respiration (R_E) from SiBCASA.

3. **Further Reading**

- **van der Velde, I. R. *et al.* (2013)**, Biosphere model simulations of interannual variability in terrestrial $^{13}C/^{12}C$ exchange, *Global Biogeochemical Cycles*, 27(3), 637-649.
- **van der Velde, I. R. *et al.* (2014)**, Terrestrial cycling of $^{13}CO_2$ by photosynthesis, respiration, and biomass burning in SiBCASA , *Biogeosciences*, 11, 6553-6571.
- **Schaefer, K. *et al.* (2008)**, Combined simple biosphere/Carnegie-Ames-Stanford approach terrestrial carbon cycle model. *Journal of Geophysical Research: Atmospheres* , 113(G3)
- **Olsen and Randerson (2004)**, Differences between surface and column atmospheric CO_2 and implications for carbon cycle research, *Journal of Geophysical Research: Atmospheres*, 109, D2, 27
- **van der Werf, G.R. *et al.* (2006)**, Interannual variability in global biomass burning emissions from 1997 to 2004, *Atm. Chem. Phys.*, 6(11), 3423-3441

Fossil Fuel Module [go to top]

1. **Introduction**

Human beings first influenced the carbon cycle through land-use change. Early humans used fire to control animals and later cleared forest for agriculture. Over the last two centuries, following the industrial and technical revolutions and the world population increase, fossil fuel combustion has become the largest anthropogenic source of CO_2. Coal, oil and natural gas combustion indeed are the most common energy sources in both developed and developing countries. Various sectors of the economy rely on fossil fuel combustion: power generation, transportation, residential/commercial building heating, and industrial processes. In 2014, the world emissions of CO_2 from fossil fuel burning, cement manufacturing, and flaring reached 9.85 PgC and stayed almost constant in 2015 at 9.86 PgC (1 $PgC=10^{15}$ grams of carbon) [**CDIAC**]. The largest share of CO_2 emissions to the atmosphere from fossil fuel burning was in China: 29% in 2017, followed by the USA (14%), Europe/EU28 (10%) and India (7%).

2. **Detailed Description**

The fossil fuel emission inventory used in CarbonTracker Europe is the one constructed for the **CARBONES** project by **USTUTT/IER**. It uses emissions from the **EDGAR 4.2 database** together with country and sector specific time profiles derived by IER. A detailed description of the construction of the product is found **here**. The global total emissions for 2000-2017 were scaled to the global totals used in the **Global Carbon Budget 2017**. An individual trend per continent/Transcom region was applied in this scaling.

3. **Further Reading**

- **CDIAC (Marland et al.) Annual Global and National fluxes**
- **CDIAC (Blasing et al.) Monthly USA fluxes**
- **Energy Information Administration (EIA)**
- **CARBONES project**
- **EDGAR Database**
- **Institut fur Energiewirtschaft und Rationelle Energieanwendung**

Observations [go to top]

1. **Introduction**

The observations of atmospheric CO_2 mole fraction by over **40 different laboratories** are at the heart of CarbonTracker. They inform us on changes in the carbon cycle, whether they are regular (such as the seasonal growth and decay of leaves and trees), or irregular (such as the release of tons of carbon by a wildfire). The results in CarbonTracker depend directly on the quality, amount and location of observations available, and the degree of detail at which we can monitor the carbon cycle reliably increases strongly with the density of our observing network.

2. **Detailed Description**

This study uses CO_2 observations from in-situ measurements or from air samples collected in flasks at 354 global sites by 46 institutions worldwide. All contributing laboratories are included under **collaborators**. These observations are included in **ObsPack** GLOBALVIEWplusv3.2 and NRTv4.2. This ObsPack product contains 354 time series of surface flask samples, quasi-continuous in-situ observations also from towers and aircraft samples. Table 1 and the figure below summarize which time series have been used in our inversion. We assimilate a maximum of 1 time series per site (e.g. not 2 from the same location from different laboratories). Note that all of these observations are calibrated against the same world CO_2 scale (WMO-2007).

For most of the quasi-continuous sampling sites, the time series consist of hourly averaged mole fractions. We assimilate only mole fractions from the afternoon hours, recognizing that our atmospheric transport model does not always capture the continental nighttime stability regime while daytime well-mixed conditions are better matched. At mountain-top sites (e.g. MLO, NWR, and SPL), we use the mole fractions from the nighttime hours as this tends to be the most stable time period and avoids periods of upslope flows that contain local vegetative and/or anthropogenic influence. The selection of hourly observations included in the assimilation is based on the flags as set in the ObsPack data sets. A set of coastal sites is moved by one degree into the ocean to force the model sample to be more representative of the actual site conditions (based on Transcom continuous simulations). Table 1 summarizes how data from the different measurement programs are included for this study.

The CO_2 data from ObsPack used in CarbonTracker are freely available for **download**. Users are encouraged to review the literature and contact the measurement labs directly for details about and access to the actual observations.

We apply a further selection criterion during the assimilation to exclude non-marine boundary layer (MBL) and non-deep Southern Hemisphere observations that are very poorly forecasted in our framework. We use the so-called model-data mismatch (MDM) in this process, which is the random error ascribed to each observation to account for measurement errors as well as modeling errors of that observation. We scale the MDM with the amount of available observations per day, to represent both flask samples and quasi-continuous observations with equal weight. We interpret an observed-minus-forecasted (OmF) mole fraction that exceeds 3 times the prescribed model-data mismatch as an indicator that our modeling framework fails. This can happen for instance when an air sample is representative of local exchange not captured well by our 1x1 degree fluxes, when local meteorological conditions are not captured by our offline transport fields, but also when large-scale CO_2 exchange is suddenly changed (e.g. fires, pests, droughts) to an extent that can not be accommodated by our flux modules. This last situation would imply an important change in the carbon cycle and has to be recognized by the researchers when analyzing the results. In accordance with the 3-sigma rejection criterion, less than 1% of the observations are discarded through this mechanism in our assimilations.

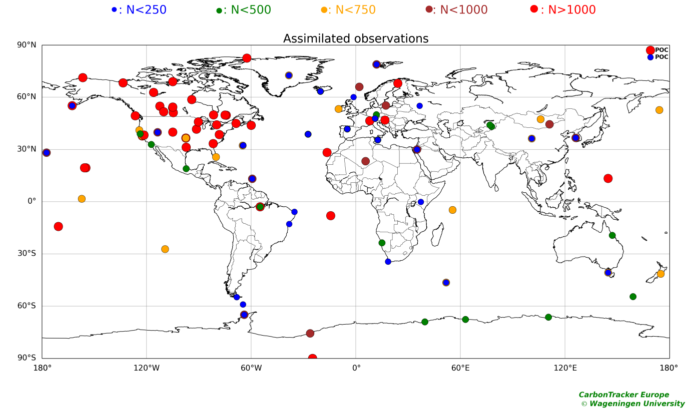

Table 1 gives a summary of the observing sites used in CarbonTracker and the assimilation performance. Model-data-mismatch ("R") is a value assigned to a given site that is meant to quantify our expected ability to simulate observations there. This value is principally determined from the limitations of the atmospheric transport model. It is part of the standard deviation used to interpret the difference between a simulation first guess ("Hx") of an observation and the actual measured value ("z"). The other component, HPH^T is a measure of the ability of the ensemble Kalman filter to improve its simulated value for this observation by adjusting fluxes. These elements together form the innovation χ statistic for the site: $\chi = (z-Hx)/\sqrt{(HPH^T+r^2)}$. The innovation χ^2 reported is the mean of all squared χ values for a given site. An average χ^2 below 1.0 indicates that the $\sqrt{(HPH^T+r^2)}$ values are too large. Conversely, values above 1.0 mean that this standard deviation is underestimated. The bias is a statistic of the posterior residuals (final modeled values - measured values). The bias is the mean of these residuals.

Table 1: Summary of observing sites used in CarbonTracker Europe and assimilation performance.

Site code	Sampling Type	Lab.	Country	Lat, Lon, Elev. (m ASL)	No. Obs. Available	No. Obs. Assimilated	√R (μmol mol^{-1})	√HPH (μmol mol^{-1})	H(x)-y (μmol mol^{-1})	H(x)-y (JJAS) (μmol mol^{-1})	H(x)-y (NDJFMA) (μmol mol^{-1})	Inn. X^2	Site code
CGO	surface-flask	NOAA	Australia	40°41'S, 144°41'E, 94 masl	591	582	+0.50	+0.12	+0.14± 0.39	+0.44± 0.30	-0.10± 0.30	+0.72	CGO
ACG	aircraft-pfp	NOAA	United States	65° 0'N, 165° 0'W, 0 masl	99	0	+1000.00	+2.90	-0.41± 3.42	-0.04± 4.04	+nan± nan	-99.00	ACG
MEX	surface-flask	NOAA	Mexico	18°59'N, 97°19'W, 4464 masl	36	36	+2.50	+0.32	+0.80± 1.16	+1.26± 1.36	+0.18± 0.61	+0.28	MEX
IZO	surface-flask	NOAA	Spain	28°19'N, 16°30'W, 2372 masl	711	0	+1000.00	+0.15	+0.58± 1.04	+0.59± 1.04	+0.58± 1.06	-99.00	IZO
HNP	surface-insitu	EC	Canada	43°37'N, 79°23'W, 87 masl	528	0	+1000.00	+10.50	-2.09±10.54	+nan± nan	-2.55±11.32	-99.00	HNP
MVY	surface-insitu	NOAA	United States	41°20'N, 70°34'W, 0 masl	63987	0	+1000.00	+4.22	+1.08± 6.63	+0.68± 9.50	+1.22± 4.80	-99.00	MVY
CPT	surface-flask	NOAA	South Africa	34°21'S, 18°29'E, 230 masl	17	17	+1.50	+0.30	+0.01± 0.80	+0.69± 0.38	-0.47± 0.76	+0.37	CPT
HIL	aircraft-pfp	NOAA	United States	40° 4'N, 87°55'W, 201 masl	2196	0	+1000.00	+2.25	-0.03± 2.42	-0.21± 3.27	+0.15± 1.72	-99.00	HIL
BHD	surface-flask	SIO_CO2	New Zealand	41°24'S, 174°52'E, 85 masl	161	0	+1000.00	+0.43	+0.70± 1.18	+1.08± 1.02	+0.39± 1.31	-99.00	BHD
ACT	aircraft-pfp	NOAA	United States	Variable	128	0	+1000.00	+5.12	-9.73±27.14	-9.73±27.14	+nan± nan	-99.00	ACT
USH	surface-flask	NOAA	Argentina	54°51'S, 68°19'W, 12 masl	243	228	+0.75	+0.17	-0.01± 0.50	-0.03± 0.47	+0.04± 0.52	+0.45	USH
ASK	surface-flask	NOAA	Algeria	23°16'N, 5°38'E, 2710 masl	41	41	+0.75	+0.16	-0.27± 0.51	-0.42± 0.43	-0.12± 0.60	+0.62	ASK
IZO	surface-flask	NOAA	Spain	28°19'N, 16°30'W, 2372 masl	46	0	+1000.00	+0.15	+0.76± 1.08	+1.09± 1.07	+0.62± 1.09	-99.00	IZO
INX02	surface-insitu	PSU	United States	39°48'N, 86° 1'W, 266 masl	10909	0	+1000.00	+9.55	-1.56± 9.31	-2.46±13.20	-1.30± 6.38	-99.00	INX02
BMW	surface-flask	NOAA	United Kingdom	32°16'N, 64°53'W, 30 masl	586	564	+1.51	+0.60	+0.61± 1.11	+0.62± 1.07	+0.61± 1.09	+0.79	BMW
Site code	**Sampling Type**	**Lab.**	**Country**	**Lat, Lon, Elev. (m ASL)**	**No. Obs. Available**	**No. Obs. Assimilated**	**√R (μmol mol^{-1})**	**√HPH (μmol mol^{-1})**	**H(x)-y (μmol mol^{-1})**	**H(x)-y (JJAS) (μmol mol^{-1})**	**H(x)-y (NDJFMA) (μmol mol^{-1})**	**Inn. X^2**	**Site code**
ALT	surface-flask	NOAA	Canada	82°27'N, 62°30'W, 190 masl	44	0	+1000.00	+0.56	+0.27± 0.75	-0.04± 0.82	+0.42± 0.65	-99.00	ALT
CRV	surface-pfp	NOAA	United States	64°59'N, 147°36'W, 611 masl	180	0	+1000.00	+2.29	+0.72± 3.56	+2.50± 4.22	-0.20± 2.01	-99.00	CRV
ALT	surface-flask	CSIRO	Canada	82°27'N, 62°30'W, 190 masl	599	0	+1000.00	+0.46	+0.16± 0.67	+0.08± 0.72	+0.28± 0.65	-99.00	ALT
UTMSA	tower-insitu	U-ATAQ	United States	40°39'N, 111°53'W, 1315 masl	22457	0	+1000.00	+5.46	-10.54±21.45	-8.13±18.32	-12.63±24.26	-99.00	UTMSA
SSL	surface-insitu	UBA-SCHAU	Germany	47°55'N, 7°55'E, 1205 masl	138848	0	+1000.27	+2.81	-0.48± 4.78	-0.05± 5.97	-0.76± 3.80	-99.00	SSL
WKT	tower-insitu	NOAA	United States	31°19'N, 97°20'W, 251 masl	112078	18423	+5.98	+2.96	+0.04± 2.46	-0.04± 2.40	+0.11± 2.48	+0.25	WKT
RBA	surface-insitu	NCAR	United States	36°28'N, 109° 6'W, 2982 masl	25269	0	+1000.00	+0.35	-0.02± 1.19	-0.04± 1.37	-0.05± 1.13	-99.00	RBA

ETL	aircraft-pfp	NOAA	Canada	54°21'N, 104°59'W, 492 masl	2764	0	+1000.00	+1.33	+0.35± 1.87	+0.99± 2.66	+0.07± 1.09	-99.00	ETL
SGP	aircraft-pfp	NOAA	United States	36°36'N, 97°29'W, 314 masl	6218	0	+1000.00	+2.48	+0.19± 2.52	+0.09± 3.06	+0.35± 1.74	-99.00	SGP
SNP	tower-insitu	NOAA	United States	38°37'N, 78°21'W, 1008 masl	64197	10421	+7.93	+3.72	+0.12± 4.05	+1.68± 4.76	-0.94± 3.29	+0.41	SNP
PAL	surface-flask	NOAA	Finland	67°58'N, 24° 7'E, 565 masl	656	0	+1000.00	+2.58	-0.48± 3.55	-0.55± 4.35	-0.37± 3.20	-99.00	PAL
BGI	aircraft-pfp	NOAA	United States	42°49'N, 94°25'W, 355 masl	357	0	+1000.00	+2.77	+0.31± 2.89	+0.55± 3.91	+0.24± 1.59	-99.00	BGI
CAR	aircraft-pfp	NOAA	United States	40°38'N, 104°20'W, 1488 masl	228	0	+1000.00	+0.80	-0.01± 2.26	+0.02± 2.30	+0.19± 1.34	-99.00	CAR
SSC	surface-insitu	ICTA-UAB	Spain	38°18'N, 2°35'W, 1349 masl	16769	0	+1000.00	+0.95	+0.19± 3.45	-0.74± 3.15	+1.49± 3.02	-99.00	SSC
SMO	surface-insitu	NOAA	American Samoa	14°15'S, 170°34'W, 42 masl	128879	17885	+1.41	+0.11	-0.10± 0.52	+0.26± 0.35	-0.41± 0.46	+0.18	SMO
Site code	**Sampling Type**	**Lab.**	**Country**	**Lat, Lon, Elev. (m ASL)**	**No. Obs. Available**	**No. Obs. Assimilated**	**√R (μmol mol^{-1})**	**√HPH (μmol mol^{-1})**	**H(x)-y (μmol mol^{-1})**	**H(x)-y (JJAS) (μmol mol^{-1})**	**H(x)-y (NDJFMA) (μmol mol^{-1})**	**Inn. χ^2**	**Site code**
HUN	tower-insitu	HMS	Hungary	46°57'N, 16°39'E, 248 masl	125871	0	+1000.00	+10.34	-1.19± 8.20	-2.19± 9.61	-0.27± 6.95	-99.00	HUN
AMT	tower-insitu	NOAA	United States	45° 2'N, 68°41'W, 53 masl	102601	16833	+5.97	+7.79	+0.06± 2.50	+0.47± 3.26	-0.19± 1.90	+0.26	AMT
LEW	surface-pfp	NOAA	United States	40°57'N, 76°53'W, 161 masl	333	0	+1000.00	+6.21	-0.87± 7.62	-1.45±10.16	-0.57± 5.16	-99.00	LEW
HIP	aircraft-insitu	HU	United States	Variable	130016	0	+1000.00	+0.47	+0.10± 1.25	+0.29± 1.33	-0.09± 1.14	-99.00	HIP
SMO	surface-flask	SIO	American Samoa	14°15'S, 170°34'W, 42 masl	466	0	+1000.00	+0.11	-0.16± 0.79	+0.23± 0.57	-0.48± 0.83	-99.00	SMO
SYO	surface-flask	NOAA	Japan	69° 1'S, 39°35'E, 14 masl	2	2	+0.50	+0.10	-0.30± 0.17	+nan± nan	-0.30± 0.17	+0.49	SYO
CMA	aircraft-pfp	NOAA	United States	38°50'N, 74°19'W, 0 masl	174	0	+1000.00	+1.73	-0.16± 3.18	-0.54± 4.27	-0.01± 1.45	-99.00	CMA
GPA	surface-flask	CSIRO	Australia	12°15'S, 131° 3'E, 25 masl	59	0	+1000.00	+0.96	+1.14± 2.76	+1.22± 2.66	+0.96± 2.41	-99.00	GPA
AMT	surface-pfp	NOAA	United States	45° 2'N, 68°41'W, 53 masl	1307	0	+1000.00	+4.11	-0.29± 2.63	-0.06± 3.61	-0.39± 2.04	-99.00	AMT
VAC	surface-insitu	ICTA-UAB	Spain	42°53'N, 3°13'W, 1102 masl	17896	0	+1000.00	+2.20	-0.79± 3.47	-1.12± 4.56	-0.32± 2.50	-99.00	VAC
CGO	surface-flask	SIO	Australia	40°41'S, 144°41'E, 94 masl	347	0	+1000.00	+0.12	+0.34± 0.40	+0.65± 0.29	+0.10± 0.31	-99.00	CGO
FWI	aircraft-pfp	NOAA	United States	44°40'N, 90°58'W, 334 masl	378	0	+1000.00	+2.52	+0.17± 2.99	-0.05± 3.67	+0.73± 2.72	-99.00	FWI
OMP	surface-insitu	OSU	United States	44°30'N, 123°33'W, 1249 masl	88898	0	+1000.00	+1.48	+1.14± 3.31	+2.01± 4.31	+0.56± 2.11	-99.00	OMP
RGL	tower-insitu	UNIVBRIS	United Kingdom	51°60'N, 2°32'W, 204 masl	32310	0	+1000.00	+5.56	-0.98± 6.99	-2.16± 8.16	+0.34± 5.63	-99.00	RGL
WGC	surface-pfp	NOAA	United States	38°16'N, 121°29'W, 0 masl	2036	0	+1000.00	+8.63	-1.93± 9.00	+1.87± 7.52	-4.63± 9.77	-99.00	WGC
Site code	**Sampling Type**	**Lab.**	**Country**	**Lat, Lon, Elev. (m ASL)**	**No. Obs. Available**	**No. Obs. Assimilated**	**√R (μmol mol^{-1})**	**√HPH (μmol mol^{-1})**	**H(x)-y (μmol mol^{-1})**	**H(x)-y (JJAS) (μmol mol^{-1})**	**H(x)-y (NDJFMA) (μmol mol^{-1})**	**Inn. χ^2**	**Site code**
SGP	aircraft-pfp	NOAA	United States	36°36'N, 97°29'W, 314 masl	35	0	+1000.00	+2.20	-0.27± 1.16	+nan± nan	-0.02± 1.16	-99.00	SGP
CHM	surface-insitu	EC	Canada	49°41'N, 74°18'W, 393 masl	24321	4183	+5.33	+3.97	-0.05± 2.08	+0.57± 2.48	-0.23± 2.00	+0.25	CHM
ZEP	surface-insitu	NILU	Norway and Sweden	78°54'N, 11°53'E, 474 masl	8346	0	+1000.00	+0.52	+0.45± 1.20	-0.10± 1.32	+0.76± 1.09	-99.00	ZEP
TOM	aircraft-insitu	NOAA	United States	Variable	23993	0	+1000.00	+0.66	-0.45± 1.30	-0.45± 1.30	+nan± nan	-99.00	TOM
ACR	surface-insitu	PSU	United States	35°56'N, 84°20'W, 372 masl	9073	0	+1000.00	+15.56	-3.10±17.43	-6.23±22.73	-1.32±11.92	-99.00	ACR
SCT	tower-insitu	NOAA	United States	33°24'N, 81°50'W, 115 masl	69039	11240	+5.96	+5.40	+0.07± 3.15	+0.13± 3.53	-0.09± 2.90	+0.43	SCT
CON	aircraft-insitu	NIES	Multiple	Variable	2754808	0	+1018.91	+0.34	+0.15± 1.54	-0.00± 1.78	+0.20± 1.37	-99.00	CON
ACG	aircraft-pfp	NOAA	United States	Variable	1545	0	+1000.00	+1.17	+0.13± 2.03	+0.24± 2.38	+0.35± 1.36	-99.00	ACG
SONGNEX2015	aircraft-insitu	NOAA-CSD	United States	Variable	42659	0	+1000.00	+1.95	+0.18± 2.00	+nan± nan	+0.18± 2.00	-99.00	SONGNEX2015
BCK	surface-insitu	EC	Canada	62°48'N, 116° 3'W, 179 masl	43728	7767	+5.49	+3.17	+0.03± 1.58	-0.10± 2.55	+0.09± 1.19	+0.15	BCK
LARC	aircraft-insitu	NASA-LaRC	United States	Variable	21114	0	+1000.00	+0.84	-2.18±15.27	-2.18±15.27	+nan± nan	-99.00	LARC
PV	surface-insitu	CALTECH	United States	33°45'N, 118°21'W, 320 masl	25337	0	+1000.00	+1.93	+9.20±12.06	+10.03± 9.11	+8.48±13.69	-99.00	PV
MRC	tower-insitu	PSU	United States	41°42'N, 76° 0'W, -9999999999999999455752309870428160 masl	66938	0	+1000.00	+8.34	-2.37± 8.44	-3.64±10.86	-1.12± 5.25	-99.00	MRC
BRW	surface-insitu	NOAA	United States	71°19'N, 156°37'W, 11 masl	135839	15197	+1.36	+1.42	+0.13± 0.67	+0.32± 0.79	+0.02± 0.61	+0.72	BRW
TAB	aircraft-pfp	IPEN	Brazil	5°57'S, 70° 4'W, -9999999999999999455752309870428160 masl	463	0	+1000.00	+0.87	-0.09± 3.61	-0.21± 4.83	+0.04± 1.91	-99.00	TAB
Site code	**Sampling Type**	**Lab.**	**Country**	**Lat, Lon, Elev. (m ASL)**	**No. Obs. Available**	**No. Obs. Assimilated**	**√R (μmol mol^{-1})**	**√HPH (μmol mol^{-1})**	**H(x)-y (μmol mol^{-1})**	**H(x)-y (JJAS) (μmol mol^{-1})**	**H(x)-y (NDJFMA) (μmol mol^{-1})**	**Inn. χ^2**	**Site code**
NWR	surface-insitu	NCAR	United States	40° 3'N, 105°35'W, 3523 masl	72734	0	+1000.00	+0.53	+0.07± 1.61	+0.25± 2.11	-0.00± 1.18	-99.00	NWR
BNE	aircraft-pfp	NOAA	United States	40°48'N, 97°11'W, 465 masl	1080	0	+1000.00	+2.29	+0.14± 3.19	+0.41± 3.37	+0.34± 1.84	-99.00	BNE
UTMUR	tower-insitu	U-ATAQ	United States	40°39'N, 111°53'W, 1315 masl	68796	0	+1000.00	+4.88	-23.88±32.49	-17.42±23.19	-29.44±38.05	-99.00	UTMUR
NHA	aircraft-pfp	NOAA	United States	42°57'N, 70°38'W, 0 masl	98	0	+1000.00	+1.92	+0.37± 2.23	+0.41± 2.63	+0.46± 0.96	-99.00	NHA
SMR	tower-insitu	UHELS	Finland	61°51'N, 24°18'E, 181 masl	31099	0	+1000.00	+5.34	-0.58± 6.70	-2.56± 9.10	+0.84± 4.94	-99.00	SMR

MKN	surface-flask	NOAA	Kenya	0° 4'S, 37°18'E, 3644 masl	138	138	+2.50	+0.22	+1.62± 1.97	+2.35± 2.18	+1.28± 1.54	+1.05	MKN
CAR	aircraft-pfp	NOAA	United States	40°38'N, 104°20'W, 1488 masl	5474	0	+1000.00	+0.47	+0.37± 1.12	+0.20± 1.34	+0.54± 0.90	-99.00	CAR
TAC	surface-flask	NOAA	United Kingdom	52°31'N, 1° 8'E, 56 masl	48	0	+1000.00	+2.63	+0.59± 5.42	+2.26± 4.39	-1.46± 6.25	-99.00	TAC
HUN	tower-insitu	HMS	Hungary	46°57'N, 16°39'E, 248 masl	125564	0	+1000.00	+11.11	-8.07±16.93	-13.52±22.71	-3.91±10.18	-99.00	HUN
ACT	aircraft-insitu	NASA-LaRC	United States	Variable	82471	0	+1000.00	+4.12	-1.29± 4.60	-1.29± 4.60	+nan± nan	-99.00	ACT
INX05	surface-insitu	PSU	United States	39°54'N, 86°12'W, 251 masl	5880	0	+1000.00	+12.84	-1.58±13.83	-2.30±15.67	-0.93±10.25	-99.00	INX05
ALT	surface-insitu	EC	Canada	82°27'N, 62°30'W, 190 masl	130468	25148	+1.64	+0.45	+0.08± 0.62	+0.03± 0.70	+0.12± 0.60	+0.27	ALT
GCI04	tower-insitu	PSU	United States	33°11'N, 85°53'W, 328 masl	11596	0	+1000.00	+6.25	-1.63± 7.89	-2.63± 8.36	-1.28± 7.72	-99.00	GCI04
INX09	surface-insitu	PSU	United States	39°52'N, 85°45'W, 277 masl	4739	0	+1000.00	+10.63	-2.03±12.83	-2.92±15.68	-0.64± 6.75	-99.00	INX09
LARC	aircraft-insitu	NASA-LaRC	United States	Variable	25077	0	+1000.00	+2.64	-2.82± 8.45	-2.82± 8.45	+nan± nan	-99.00	LARC
Site code	**Sampling Type**	**Lab.**	**Country**	**Lat, Lon, Elev. (m ASL)**	**No. Obs. Available**	**No. Obs. Assimilated**	**√R (μmol mol^{-1})**	**√HPH (μmol mol^{-1})**	**H(x)-y (μmol mol^{-1})**	**H(x)-y (JJAS) (μmol mol^{-1})**	**H(x)-y (NDJFMA) (μmol mol^{-1})**	**Inn. χ^2**	**Site code**
KUM	surface-flask	SIO_CO2	United States	19°31'N, 154°49'W, 3 masl	862	0	+1000.00	+0.11	-0.34± 2.00	-0.37± 2.06	-0.27± 1.92	-99.00	KUM
WBI	tower-insitu	NOAA	United States	41°43'N, 91°21'W, 241 masl	9312	1430	+6.00	+6.48	-0.08± 3.34	+0.34± 4.22	-0.32± 2.80	+0.61	WBI
SAM	aircraft-pfp	NOAA	United States	Variable	119	0	+1000.00	+0.93	-0.12± 1.69	+nan± nan	-0.12± 1.69	-99.00	SAM
CHL	surface-insitu	EC	Canada	58°45'N, 94° 4'W, 29 masl	2419	500	+5.63	+2.21	+0.51± 0.97	+nan± nan	+0.51± 0.97	+0.07	CHL
WKT	surface-pfp	NOAA	United States	31°19'N, 97°20'W, 251 masl	148	0	+1000.00	+3.38	-0.35± 2.87	+0.21± 2.63	-0.67± 3.13	-99.00	WKT
THD	surface-flask	NOAA	United States	41° 3'N, 124° 9'W, 107 masl	21	21	+5.00	+0.38	+1.08± 1.01	+1.84± 0.00	+1.05± 0.95	+0.09	THD
SPO	surface-flask	SIO_CO2	United States	89°59'S, 24°48'W, 2810 masl	412	0	+1000.00	+0.10	-0.02± 1.29	+0.22± 0.80	-0.13± 0.78	-99.00	SPO
CON	aircraft-flask	NIES	Multiple	Variable	3655	0	+1000.00	+0.14	-0.02± 0.76	+0.12± 0.66	-0.11± 0.78	-99.00	CON
NMB	surface-flask	NOAA	Namibia	23°35'S, 15° 2'E, 456 masl	39	39	+1.50	+0.59	+0.45± 1.38	+0.82± 0.84	-0.71± 1.08	+0.94	NMB
DND	aircraft-pfp	NOAA	United States	47°30'N, 99°14'W, 472 masl	2123	0	+1000.00	+1.72	+0.32± 2.29	+0.87± 3.33	+0.11± 1.35	-99.00	DND
ACT	aircraft-insitu	NASA-LaRC	United States	Variable	135475	0	+1000.07	+3.56	+0.45± 3.46	+nan± nan	+0.56± 2.69	-99.00	ACT
CRV	tower-insitu	NOAA	United States	64°59'N, 147°36'W, 611 masl	9035	0	+1000.00	+2.52	+0.27± 3.32	+1.09± 4.70	+0.03± 2.07	-99.00	CRV
KZM	surface-flask	NOAA	Kazakhstan	43°15'N, 77°53'E, 2519 masl	411	391	+2.50	+0.92	+0.12± 2.23	+0.67± 2.09	-0.61± 1.80	+0.84	KZM
WBI	surface-pfp	NOAA	United States	41°43'N, 91°21'W, 241 masl	2112	0	+1000.00	+6.49	-0.14± 4.30	+0.31± 6.22	-0.40± 2.53	-99.00	WBI
LARC	aircraft-insitu	NASA-LaRC	United States	Variable	42014	0	+1000.00	+0.98	-1.33± 1.10	-1.33± 1.10	+nan± nan	-99.00	LARC
Site code	**Sampling Type**	**Lab.**	**Country**	**Lat, Lon, Elev. (m ASL)**	**No. Obs. Available**	**No. Obs. Assimilated**	**√R (μmol mol^{-1})**	**√HPH (μmol mol^{-1})**	**H(x)-y (μmol mol^{-1})**	**H(x)-y (JJAS) (μmol mol^{-1})**	**H(x)-y (NDJFMA) (μmol mol^{-1})**	**Inn. χ^2**	**Site code**
WAO	surface-insitu	UEA	United Kingdom	52°57'N, 1° 7'E, 20 masl	51100	0	+1000.00	+4.61	-1.92± 7.17	-2.91± 8.27	-1.14± 6.14	-99.00	WAO
HFM	aircraft-pfp	NOAA	United States	42°32'N, 72°10'W, 340 masl	1620	0	+1000.00	+2.06	+0.46± 2.45	+0.36± 3.72	+0.42± 1.55	-99.00	HFM
UTDBK	tower-insitu	U-ATAQ	United States	40°32'N, 112° 4'W, 1583 masl	69223	0	+1000.00	+1.73	-2.33± 7.46	-2.48± 6.36	-2.25± 8.55	-99.00	UTDBK
SPO	surface-flask	NOAA	United States	89°59'S, 24°48'W, 2810 masl	874	0	+1000.00	+0.09	+0.15± 0.29	+0.40± 0.21	-0.02± 0.23	-99.00	SPO
INX07	surface-insitu	PSU	United States	39°46'N, 86°16'W, 241 masl	6391	0	+1000.00	+13.96	-5.21±15.54	-6.70±17.58	-4.02±11.98	-99.00	INX07
LEF	surface-pfp	NOAA	United States	45°57'N, 90°16'W, 472 masl	151	0	+1000.00	+4.78	-0.56± 2.71	-1.32± 3.97	-0.22± 1.50	-99.00	LEF
SCA	aircraft-pfp	NOAA	United States	32°46'N, 79°33'W, 0 masl	107	0	+1000.00	+1.18	+0.28± 1.52	+0.49± 3.17	+0.35± 0.90	-99.00	SCA
UUM	surface-flask	NOAA	Mongolia	44°27'N, 111° 6'E, 1007 masl	39	39	+2.50	+1.18	+0.03± 1.52	-0.22± 1.15	-0.12± 1.30	+0.43	UUM
CHR	surface-flask	NOAA	Republic of Kiribati	1°42'N, 157° 9'W, 0 masl	5	5	+0.75	+0.20	-0.28± 0.54	-0.28± 0.54	+nan± nan	+0.36	CHR
ESP	surface-flask	CSIRO	Canada	49°23'N, 126°33'W, 7 masl	28	0	+1000.00	+0.82	-0.10± 1.77	+1.00± 1.37	-1.19± 1.53	-99.00	ESP
RYO	surface-insitu	JMA	Japan	39° 2'N, 141°49'E, 260 masl	66898	0	+1000.00	+1.34	-0.27± 2.42	+0.48± 3.62	-0.21± 1.79	-99.00	RYO
BHD	surface-flask	NOAA	New Zealand	41°24'S, 174°52'E, 85 masl	8	8	+0.75	+0.16	-0.23± 0.64	+0.18± 0.17	-0.60± 0.72	+0.83	BHD
WKT	surface-pfp	NOAA	United States	31°19'N, 97°20'W, 251 masl	2107	0	+1000.00	+3.33	-0.23± 2.98	-0.21± 3.30	-0.18± 2.65	-99.00	WKT
ACT	aircraft-insitu	NASA-LaRC	United States	Variable	70367	0	+1000.00	+4.63	-1.46± 6.56	-1.46± 6.56	+nan± nan	-99.00	ACT
ALT	surface-flask	SIO_CO2	Canada	82°27'N, 62°30'W, 190 masl	716	0	+1000.00	+0.49	-0.74± 6.68	-0.32± 1.55	-1.24± 9.37	-99.00	ALT
Site code	**Sampling Type**	**Lab.**	**Country**	**Lat, Lon, Elev. (m ASL)**	**No. Obs. Available**	**No. Obs. Assimilated**	**√R (μmol mol^{-1})**	**√HPH (μmol mol^{-1})**	**H(x)-y (μmol mol^{-1})**	**H(x)-y (JJAS) (μmol mol^{-1})**	**H(x)-y (NDJFMA) (μmol mol^{-1})**	**Inn. χ^2**	**Site code**
NMB	surface-flask	NOAA	Namibia	23°35'S, 15° 2'E, 456 masl	376	359	+1.50	+0.51	-0.15± 1.18	+0.41± 0.94	-0.76± 1.06	+0.72	NMB
STM	surface-flask	NOAA	Norway	66° 0'N, 2° 0'E, 0 masl	907	849	+1.50	+0.94	+0.09± 0.98	+0.25± 1.04	+0.01± 0.94	+0.53	STM
CHR	surface-flask	SIO_CO2	Republic of Kiribati	1°42'N, 157° 9'W, 0 masl	485	0	+1000.00	+0.15	-2.21± 7.38	-1.68± 3.81	-2.42± 9.23	-99.00	CHR
MBO	surface-pfp	NOAA	United States	43°59'N, 121°41'W, 2731 masl	161	0	+1000.00	+0.77	-0.04± 1.84	+0.01± 2.41	-0.06± 1.04	-99.00	MBO

PDM	surface-flask	LSCE	France	42°56'N, 0° 8'E, 2877 masl	389	0	+1000.00	+0.42	-0.56± 2.27	-0.08± 2.35	-0.87± 2.11	-99.00	PDM
UTRPK	tower-insitu	U-ATAQ	United States	40°48'N, 111°56'W, 1288 masl	44324	0	+1000.00	+4.71	-22.54±32.14	-20.26±26.98	-25.83±38.33	-99.00	UTRPK
MQA	surface-flask	CSIRO	Australia	54°29'S, 158°58'E, 6 masl	493	493	+0.58	+0.15	+0.04± 0.41	+0.25± 0.43	-0.11± 0.34	+0.61	MQA
TTA	tower-insitu	UNIVBRIS	United Kingdom	56°33'N, 2°59'W, 400 masl	18693	0	+1000.00	+1.20	-0.14± 3.12	+0.29± 3.58	-0.41± 2.57	-99.00	TTA
FNE	surface-insitu	EC	Canada	58°50'N, 122°34'W, 361 masl	3459	0	+1000.00	+4.81	-1.46± 7.13	+nan± nan	-0.68± 5.94	-99.00	FNE
NWR	surface-flask	NOAA	United States	40° 3'N, 105°35'W, 3523 masl	816	0	+1000.00	+0.52	+0.42± 1.80	+1.46± 1.98	-0.18± 1.40	-99.00	NWR
BIR	surface-insitu	NILU	Norway	58°23'N, 8°15'E, 219 masl	8673	0	+1000.00	+12.37	-2.66±13.33	-7.67±18.81	+0.03± 6.69	-99.00	BIR
USH	surface-flask	NOAA	Argentina	54°51'S, 68°19'W, 12 masl	33	33	+0.75	+0.20	-0.20± 0.97	-0.05± 0.43	-0.06± 0.89	+1.75	USH
INU	surface-insitu	EC	Canada	68°19'N, 133°32'W, 113 masl	3758	771	+5.61	+3.13	+0.22± 1.08	-0.28± 0.80	+0.34± 1.04	+0.10	INU
MBO	surface-pfp	NOAA	United States	43°59'N, 121°41'W, 2731 masl	869	0	+1000.00	+0.81	-0.26± 1.72	-0.42± 1.95	-0.14± 1.36	-99.00	MBO
SMO	surface-insitu	NOAA	American Samoa	14°15'S, 170°34'W, 42 masl	8736	1160	+1.43	+0.11	-0.20± 0.65	+0.40± 0.27	-0.67± 0.51	+0.25	SMO
Site code	**Sampling Type**	**Lab.**	**Country**	**Lat, Lon, Elev. (m ASL)**	**No. Obs. Available**	**No. Obs. Assimilated**	**√R ($\mu mol\ mol^{-1}$)**	**√HPH ($\mu mol\ mol^{-1}$)**	**H(x)-y ($\mu mol\ mol^{-1}$)**	**H(x)-y (JJAS) ($\mu mol\ mol^{-1}$)**	**H(x)-y (NDJFMA) ($\mu mol\ mol^{-1}$)**	**Inn. χ^2**	**Site code**
AOZ	surface-insitu	PSU	United States	38°45'N, 92°12'W, 219 masl	21628	0	+1000.00	+13.17	-2.28±12.48	-7.55±19.30	+0.75± 8.10	-99.00	AOZ
NWR	surface-flask	NOAA	United States	40° 3'N, 105°35'W, 3523 masl	46	0	+1000.00	+0.51	+0.73± 1.70	+1.79± 1.65	-0.04± 1.16	-99.00	NWR
PAL	surface-insitu	FMI	Finland	67°58'N, 24° 7'E, 565 masl	95920	0	+1000.00	+2.49	-0.25± 2.84	+0.05± 3.76	-0.22± 2.26	-99.00	PAL
OYQ	surface-insitu	OSU	United States	44°40'N, 124° 4'W, 116 masl	35249	0	+1000.00	+4.81	-0.62± 7.04	-2.38± 5.52	+0.40± 7.87	-99.00	OYQ
ALT	surface-flask	NOAA	Canada	82°27'N, 62°30'W, 190 masl	949	0	+1000.00	+0.50	+0.08± 0.81	-0.02± 0.81	+0.14± 0.71	-99.00	ALT
PSA	surface-flask	NOAA	United States	64°55'S, 64° 0'W, 10 masl	811	802	+0.50	+0.29	+0.01± 0.29	+0.12± 0.28	-0.04± 0.26	+0.38	PSA
MLO	surface-flask	NOAA	United States	19°32'N, 155°35'W, 3397 masl	55	0	+1000.00	+0.11	+0.42± 0.64	+0.27± 0.43	+0.60± 0.82	-99.00	MLO
ONG	surface-insitu	OSU	United States	43°28'N, 119°41'W, 1398 masl	80497	0	+1000.00	+2.33	-0.51± 3.71	-0.71± 4.26	-0.36± 2.99	-99.00	ONG
MRC	aircraft-pfp	NOAA	United States	41°42'N, 76° 0'W, -9999999999999999455752309870428160 masl	77	0	+1000.00	+6.49	+5.51± 4.91	+11.99± 6.12	+nan± nan	-99.00	MRC
KUM	surface-flask	SIO	United States	19°31'N, 154°49'W, 3 masl	567	0	+1000.00	+0.11	+0.07± 1.05	+0.11± 1.01	+0.09± 1.13	-99.00	KUM
SMR	tower-insitu	UHELS	Finland	61°51'N, 24°18'E, 181 masl	31192	0	+1000.00	+5.07	+0.00± 5.84	-1.19± 7.79	+1.01± 4.53	-99.00	SMR
MLO	surface-insitu	NOAA	United States	19°32'N, 155°35'W, 3397 masl	135512	16990	+1.42	+0.10	+0.17± 0.59	-0.06± 0.55	+0.31± 0.59	+0.23	MLO
SMO	surface-flask	NOAA	American Samoa	14°15'S, 170°34'W, 42 masl	1356	0	+1000.00	+0.11	-0.20± 1.30	+0.07± 1.95	-0.47± 0.76	-99.00	SMO
ASK	surface-flask	NOAA	Algeria	23°16'N, 5°38'E, 2710 masl	767	754	+0.75	+0.13	-0.09± 0.62	-0.19± 0.59	+0.00± 0.65	+0.71	ASK
LARC	aircraft-insitu	NASA-LaRC	United States	Variable	26822	0	+1000.00	+5.00	-4.64± 9.74	+nan± nan	-4.64± 9.74	-99.00	LARC
Site code	**Sampling Type**	**Lab.**	**Country**	**Lat, Lon, Elev. (m ASL)**	**No. Obs. Available**	**No. Obs. Assimilated**	**√R ($\mu mol\ mol^{-1}$)**	**√HPH ($\mu mol\ mol^{-1}$)**	**H(x)-y ($\mu mol\ mol^{-1}$)**	**H(x)-y (JJAS) ($\mu mol\ mol^{-1}$)**	**H(x)-y (NDJFMA) ($\mu mol\ mol^{-1}$)**	**Inn. χ^2**	**Site code**
BRM	tower-insitu	KUP	Switzerland	47°11'N, 8°11'E, 797 masl	33427	0	+1000.00	+6.69	+2.17± 8.64	+0.68± 9.88	+3.19± 7.71	-99.00	BRM
NWR	surface-pfp	NOAA	United States	40° 3'N, 105°35'W, 3523 masl	314	0	+1000.00	+0.66	+0.54± 2.00	+1.65± 2.29	+0.05± 1.47	-99.00	NWR
ETL	surface-insitu	EC	Canada	54°21'N, 104°59'W, 492 masl	91947	15100	+5.42	+7.26	-0.07± 2.00	-0.05± 2.85	-0.05± 1.60	+0.27	ETL
COB	aircraft-insitu	HU	N/A	Variable	22629	0	+1000.00	+2.43	+0.54± 2.80	+0.62± 3.10	+nan± nan	-99.00	COB
TEXAQS2006	aircraft-insitu	NOAA-CSD	United States	Variable	32654	0	+1000.00	+3.08	-1.71± 7.82	-1.17± 4.95	+nan± nan	-99.00	TEXAQS2006
ZEP	surface-flask	NOAA	Norway and Sweden	78°54'N, 11°53'E, 474 masl	896	856	+1.50	+0.57	+0.16± 0.88	+0.31± 0.97	+0.02± 0.84	+0.47	ZEP
DRP	shipboard-flask	NOAA	N/A	59° 0'S, 64°41'W, 0 masl	7	7	+0.50	+0.17	-0.05± 0.26	+0.41± 0.00	-0.18± 0.16	+0.55	DRP
PAL	surface-flask	NOAA	Finland	67°58'N, 24° 7'E, 565 masl	33	0	+1000.00	+2.49	-0.62± 3.80	-1.55± 5.08	+0.47± 1.70	-99.00	PAL
SENEX2013	aircraft-insitu	NOAA-CSD	United States	Variable	39612	0	+1000.00	+5.00	+0.30± 9.76	+0.32± 9.85	+nan± nan	-99.00	SENEX2013
CPT	surface-flask	NOAA	South Africa	34°21'S, 18°29'E, 230 masl	148	142	+1.52	+0.32	+0.05± 0.66	+0.46± 0.56	-0.25± 0.58	+0.21	CPT
INU	surface-insitu	EC	Canada	68°19'N, 133°32'W, 113 masl	40567	7329	+5.48	+3.76	-0.12± 1.72	-0.35± 2.51	+0.03± 1.20	+0.21	INU
KCMP	tower-insitu	UofMN	United States	44°41'N, 93° 4'W, 290 masl	9040	0	+1000.00	+7.18	-0.53± 7.52	-1.37±10.26	+0.14± 4.93	-99.00	KCMP
BRM	tower-insitu	KUP	Switzerland	47°11'N, 8°11'E, 797 masl	33399	0	+1000.00	+9.09	-0.52±11.79	-2.14±12.55	+0.50±11.20	-99.00	BRM
SUM	surface-flask	NOAA	Greenland	72°36'N, 38°25'W, 3209 masl	739	721	+0.75	+0.24	+0.11± 0.70	+0.37± 0.75	-0.05± 0.66	+1.08	SUM
WLG	surface-flask	NOAA	Peoples Republic of China	36°17'N, 100°54'E, 3810 masl	710	656	+1.53	+0.92	+0.02± 1.36	+0.16± 1.42	+0.20± 1.24	+0.86	WLG
Site code	**Sampling Type**	**Lab.**	**Country**	**Lat, Lon, Elev. (m ASL)**	**No. Obs. Available**	**No. Obs. Assimilated**	**√R ($\mu mol\ mol^{-1}$)**	**√HPH ($\mu mol\ mol^{-1}$)**	**H(x)-y ($\mu mol\ mol^{-1}$)**	**H(x)-y (JJAS) ($\mu mol\ mol^{-1}$)**	**H(x)-y (NDJFMA) ($\mu mol\ mol^{-1}$)**	**Inn. χ^2**	**Site code**
HTM	tower-insitu	LUND-CEC	Sweden	56° 6'N, 13°25'E, 115 masl	6783	0	+1000.00	+4.17	-3.00± 7.43	-4.31± 9.92	-2.10± 4.92	-99.00	HTM
BRM	tower-insitu	KUP	Switzerland	47°11'N, 8°11'E, 797 masl	33190	0	+1000.00	+7.55	+1.29± 9.80	-0.12±10.71	+2.24± 9.14	-99.00	BRM

CBY	surface-insitu	EC	Canada	69° 1'N, 105° 3'W, 35 masl	3245	633	+5.53	+2.15	+0.15± 0.78	+nan± nan	+0.12± 0.79	+0.05	CBY
BAL	surface-flask	NOAA	Poland	55°21'N, 17°13'E, 3 masl	1004	964	+5.02	+4.52	-0.95± 3.53	-1.17± 3.88	-0.82± 3.36	+0.49	BAL
HPB	surface-insitu	HPB	Germany	47°48'N, 11° 1'E, 934 masl	11475	0	+1000.00	+8.89	+1.55± 8.88	+0.68±10.70	+2.57± 6.37	-99.00	HPB
EST	surface-insitu	EC	Canada	51°40'N, 110°12'W, 707 masl	3452	579	+5.38	+5.18	+0.13± 1.87	+nan± nan	+0.14± 1.83	+0.28	EST
ICE	surface-flask	NOAA	Iceland	63°24'N, 20°17'W, 118 masl	473	439	+1.50	+0.45	-0.12± 0.78	+0.07± 0.92	-0.23± 0.68	+0.30	ICE
RKW	surface-insitu	PSU	United States	41°17'N, 89°58'W, 247 masl	16243	0	+1000.00	+7.91	-1.48± 8.47	-2.43±10.96	+0.69± 4.51	-99.00	RKW
WKT	tower-insitu	NOAA	United States	31°19'N, 97°20'W, 251 masl	8646	1355	+5.97	+3.00	-0.00± 2.63	+0.16± 2.60	-0.04± 2.70	+0.34	WKT
KZD	surface-flask	NOAA	Kazakhstan	44° 5'N, 76°52'E, 595 masl	451	425	+2.50	+2.25	-0.35± 2.49	-0.86± 2.86	-0.05± 2.00	+1.04	KZD
MID	surface-flask	NOAA	United States	28°13'N, 177°23'W, 11 masl	786	773	+1.50	+0.21	+0.60± 0.96	+0.98± 0.96	+0.44± 0.94	+0.62	MID
LARC	aircraft-insitu	NASA-LaRC	United States	Variable	50121	0	+1000.00	+0.47	+0.61± 1.79	+nan± nan	+0.61± 1.79	-99.00	LARC
IZO	surface-insitu	AEMET	Spain	28°19'N, 16°30'W, 2372 masl	125005	65386	+2.56	+0.15	+0.05± 0.77	+0.02± 0.83	+0.09± 0.78	+0.10	IZO
EIC	surface-flask	NOAA	Chile	27°10'S, 109°26'W, 47 masl	14	14	+1.50	+0.13	-1.34± 1.02	+nan± nan	-1.34± 1.02	+1.30	EIC
LLB	surface-flask	NOAA	Canada	54°57'N, 112°27'W, 540 masl	173	0	+1000.00	+5.81	-0.33± 9.89	+1.45± 9.10	-1.14±10.86	-99.00	LLB
Site code	**Sampling Type**	**Lab.**	**Country**	**Lat, Lon, Elev. (m ASL)**	**No. Obs. Available**	**No. Obs. Assimilated**	**√R (µmol mol^{-1})**	**√HPH (µmol mol^{-1})**	**H(x)-y (µmol mol^{-1})**	**H(x)-y (JJAS) (µmol mol^{-1})**	**H(x)-y (NDJFMA) (µmol mol^{-1})**	**Inn. X^2**	**Site code**
AAO	aircraft-pfp	NOAA	United States	40° 3'N, 88°22'W, 230 masl	3202	0	+1000.00	+4.92	-0.21± 5.33	-0.43± 6.88	+0.24± 2.25	-99.00	AAO
CES	tower-insitu	ECN	the Netherlands	51°58'N, 4°56'E, -1 masl	109415	0	+1000.00	+6.11	+0.13±10.26	+0.77±10.35	-0.20±10.50	-99.00	CES
HFM	tower-insitu	HU	United States	42°32'N, 72°10'W, 340 masl	33283	0	+1000.00	+8.91	-0.91±10.77	-2.87±15.67	+0.53± 6.10	-99.00	HFM
SAN	aircraft-pfp	IPEN	Brazil	2°51'S, 54°57'W, 78 masl	1101	1075	+2.00	+0.46	-0.21± 1.71	-0.14± 1.88	-0.12± 1.63	+0.99	SAN
SMO	surface-flask	SIO_CO2	American Samoa	14°15'S, 170°34'W, 42 masl	699	0	+1000.00	+0.11	-0.43± 6.41	-0.46± 9.62	-0.61± 1.81	-99.00	SMO
PUY	surface-insitu	LSCE	France	45°46'N, 2°58'E, 1465 masl	116939	0	+1000.00	+2.30	-0.60± 4.01	+0.15± 4.97	-1.18± 3.10	-99.00	PUY
WBI	tower-insitu	NOAA	United States	41°43'N, 91°21'W, 241 masl	75264	12110	+5.94	+5.93	+0.00± 3.05	+0.38± 3.93	-0.23± 2.42	+0.49	WBI
HUN	tower-insitu	HMS	Hungary	46°57'N, 16°39'E, 248 masl	129355	0	+1000.00	+10.72	-3.10± 9.88	-5.17±12.14	-1.37± 7.66	-99.00	HUN
KUM	surface-flask	NOAA	United States	19°31'N, 154°49'W, 3 masl	1124	1011	+0.90	+0.11	+0.00± 0.96	+0.02± 0.93	+0.05± 1.03	+1.29	KUM
MHD	surface-flask	NOAA	Ireland	53°20'N, 9°54'W, 5 masl	36	33	+1.50	+1.33	+0.07± 1.17	-0.03± 1.51	+0.06± 0.65	+0.77	MHD
NOR	tower-insitu	LUND-CEC	Sweden	60° 5'N, 17°29'E, 45 masl	17242	0	+1000.00	+3.23	-1.17± 5.32	-2.35± 7.34	-0.46± 3.77	-99.00	NOR
ETL	aircraft-pfp	NOAA	Canada	54°21'N, 104°59'W, 492 masl	117	0	+1000.00	+1.64	+0.55± 2.34	+0.85± 2.80	-0.09± 0.73	-99.00	ETL
SIS	surface-flask	CSIRO	Scotland	60° 5'N, 1°15'W, 30 masl	99	97	+1.51	+0.46	+0.74± 1.09	+1.47± 1.17	+0.12± 0.69	+0.98	SIS
BKT	surface-flask	NOAA	Indonesia	0°12'S, 100°19'E, 845 masl	396	0	+1000.00	+0.58	+3.35± 4.24	+3.21± 4.98	+3.63± 3.67	-99.00	BKT
ABP	surface-flask	NOAA	Brazil	12°46'S, 38°10'W, 1 masl	108	101	+1.50	+0.42	-0.70± 0.76	-0.25± 0.38	-1.18± 0.74	+0.59	ABP
Site code	**Sampling Type**	**Lab.**	**Country**	**Lat, Lon, Elev. (m ASL)**	**No. Obs. Available**	**No. Obs. Assimilated**	**√R (µmol mol^{-1})**	**√HPH (µmol mol^{-1})**	**H(x)-y (µmol mol^{-1})**	**H(x)-y (JJAS) (µmol mol^{-1})**	**H(x)-y (NDJFMA) (µmol mol^{-1})**	**Inn. X^2**	**Site code**
ESP	surface-insitu	EC	Canada	49°23'N, 126°33'W, 7 masl	58951	8566	+5.24	+3.72	-0.83± 2.39	-0.60± 2.90	-0.79± 1.97	+0.37	ESP
CRI	surface-flask	CSIRO	India	15° 5'N, 73°50'E, 60 masl	147	0	+1000.00	+6.29	-3.67± 6.85	-0.61± 3.93	-5.99± 7.73	-99.00	CRI
AOA	aircraft-flask	JMA	Japan	Variable	1411	0	+1000.00	+0.17	+0.50± 1.01	+0.41± 1.16	+0.65± 0.96	-99.00	AOA
DVV	tower-insitu	PSU	United States	36°42'N, 79°26'W, 277 masl	2609	0	+1000.00	+5.98	-0.04± 9.54	-2.96± 9.17	+1.35± 5.16	-99.00	DVV
CPS	surface-insitu	EC	Canada	49°49'N, 74°59'W, 381 masl	2994	581	+5.49	+3.57	-0.07± 1.55	+nan± nan	-0.17± 1.53	+0.08	CPS
BGU	surface-flask	LSCE	Spain	41°58'N, 3°14'E, 11 masl	552	0	+1000.00	+2.96	+0.01± 4.45	-0.11± 4.59	+0.32± 4.16	-99.00	BGU
JFJ	surface-insitu	EMPA	Switzerland	46°33'N, 7°59'E, 3570 masl	47491	7910	+2.95	+0.79	+0.15± 1.45	+0.29± 1.31	+0.08± 1.55	+0.31	JFJ
LEW	surface-pfp	NOAA	United States	40°57'N, 76°53'W, 161 masl	119	0	+1000.00	+6.10	-2.56± 6.54	-2.81± 7.99	-3.04± 6.06	-99.00	LEW
MAA	surface-flask	CSIRO	Australia	67°37'S, 62°52'E, 32 masl	407	407	+0.57	+0.10	+0.02± 0.30	+0.25± 0.26	-0.14± 0.24	+0.33	MAA
TGC	aircraft-pfp	NOAA	United States	27°44'N, 96°52'W, 0 masl	2472	0	+1000.00	+0.73	+0.22± 1.42	+0.22± 1.35	+0.31± 1.38	-99.00	TGC
CDL	surface-insitu	EC	Canada	53°59'N, 105° 7'W, 600 masl	66546	9865	+5.30	+9.75	-0.28± 2.14	+0.18± 2.60	-0.40± 1.92	+0.29	CDL
SPO	surface-insitu	NOAA	United States	89°59'S, 24°48'W, 2810 masl	138734	22824	+0.98	+0.09	+0.06± 0.28	+0.30± 0.21	-0.12± 0.20	+0.10	SPO
HAA	aircraft-pfp	NOAA	United States	21°14'N, 158°57'W, 3 masl	1797	0	+1000.00	+0.11	+0.43± 0.85	+0.41± 0.93	+0.48± 0.74	-99.00	HAA
SNP	tower-insitu	NOAA	United States	38°37'N, 78°21'W, 1008 masl	9279	1440	+7.99	+3.82	+0.06± 4.17	+1.81± 4.85	-1.25± 3.08	+0.45	SNP
SCT	surface-pfp	NOAA	United States	33°24'N, 81°50'W, 115 masl	175	0	+1000.00	+4.06	+0.05± 3.27	+0.73± 2.81	-0.34± 3.49	-99.00	SCT
Site code	**Sampling Type**	**Lab.**	**Country**	**Lat, Lon, Elev. (m ASL)**	**No. Obs. Available**	**No. Obs. Assimilated**	**√R (µmol mol^{-1})**	**√HPH (µmol mol^{-1})**	**H(x)-y (µmol mol^{-1})**	**H(x)-y (JJAS) (µmol mol^{-1})**	**H(x)-y (NDJFMA) (µmol mol^{-1})**	**Inn. X^2**	**Site code**
SGP	surface-insitu	LBNL-ARM	United States	36°36'N, 97°29'W, 314 masl	98597	16274	+5.98	+9.80	+0.08± 2.67	+0.04± 3.02	+0.12± 2.40	+0.33	SGP

KUM	surface-flask	NOAA	United States	19°31'N, 154°49'W, 3 masl	65	65	+0.92	+0.12	+0.47± 1.36	+0.81± 0.83	+0.29± 1.69	+3.12	KUM
CRZ	surface-flask	NOAA	France	46°26'S, 51°51'E, 197 masl	659	644	+0.50	+0.15	+0.17± 0.33	+0.33± 0.29	+0.03± 0.29	+0.57	CRZ
LEF	tower-insitu	NOAA	United States	45°57'N, 90°16'W, 472 masl	9025	1395	+4.99	+4.53	+0.18± 2.21	+0.61± 2.98	-0.01± 1.60	+0.38	LEF
SGP	surface-flask	NOAA	United States	36°36'N, 97°29'W, 314 masl	45	43	+3.00	+5.11	+0.01± 1.87	-0.54± 1.67	+0.33± 1.92	+0.50	SGP
HTM	tower-insitu	LUND-CEC	Sweden	56° 6'N, 13°25'E, 115 masl	6779	0	+1000.00	+2.75	-1.26± 4.46	-1.17± 5.23	-1.42± 4.12	-99.00	HTM
LEF	aircraft-pfp	NOAA	United States	45°57'N, 90°16'W, 472 masl	189	0	+1000.00	+3.07	-0.24± 2.20	-0.23± 2.64	-0.82± 1.54	-99.00	LEF
LLB	surface-insitu	EC	Canada	54°57'N, 112°27'W, 540 masl	72146	7880	+5.22	+6.83	-0.39± 2.54	-0.45± 3.08	-0.38± 2.44	+0.52	LLB
INX03	surface-insitu	PSU	United States	39°47'N, 86°10'W, 226 masl	4540	0	+1000.00	+14.12	-8.80±17.98	-10.56±20.90	-7.33±14.51	-99.00	INX03
ALF	aircraft-pfp	IPEN	Brazil	8°55'S, 56°47'W, -9999999999999999455752309870428160 masl	684	0	+1000.00	+0.79	-0.70± 2.66	-0.02± 2.24	-0.91± 2.76	-99.00	ALF
HUAC	aircraft-insitu	HU	United States	Variable	26468	0	+1000.00	+0.86	+0.34± 1.95	+0.12± 1.77	+0.39± 1.91	-99.00	HUAC
BAO	surface-pfp	NOAA	United States	40° 3'N, 105° 0'W, 1584 masl	2671	0	+1000.00	+1.37	-2.19± 5.16	-0.89± 4.21	-3.35± 5.70	-99.00	BAO
COB	aircraft-insitu	HU	N/A	Variable	52160	0	+1000.00	+3.45	+0.29± 4.53	+0.41± 5.08	+nan± nan	-99.00	COB
PFA	aircraft-pfp	NOAA	United States	65° 4'N, 147°17'W, 210 masl	131	0	+1000.00	+1.92	+0.37± 2.36	+1.27± 2.60	-0.23± 2.62	-99.00	PFA
AMY	surface-flask	NOAA	Republic of Korea	36°32'N, 126°20'E, 85 masl	29	0	+1000.00	+3.21	+1.85± 4.35	-0.04± 5.31	+3.46± 2.38	-99.00	AMY
Site code	**Sampling Type**	**Lab.**	**Country**	**Lat, Lon, Elev. (m ASL)**	**No. Obs. Available**	**No. Obs. Assimilated**	**√R (μmol mol^{-1})**	**√HPH (μmol mol^{-1})**	**H(x)-y (μmol mol^{-1})**	**H(x)-y (JJAS) (μmol mol^{-1})**	**H(x)-y (NDJFMA) (μmol mol^{-1})**	**Inn. X^2**	**Site code**
TAP	surface-flask	NOAA	Republic of Korea	36°44'N, 126° 8'E, 16 masl	787	690	+5.51	+1.68	-0.04± 3.93	+0.66± 4.94	-0.24± 2.98	+0.56	TAP
LEF	tower-insitu	NOAA	United States	45°57'N, 90°16'W, 472 masl	131755	21726	+4.98	+4.43	+0.08± 2.20	+0.44± 2.83	-0.10± 1.70	+0.35	LEF
WGC	surface-pfp	NOAA	United States	38°16'N, 121°29'W, 0 masl	107	0	+1000.00	+5.35	-3.18± 9.78	+1.08± 3.65	-6.15±12.51	-99.00	WGC
LARC	aircraft-insitu	NASA-LaRC	United States	Variable	44812	0	+1000.00	+0.38	+0.32± 1.72	+nan± nan	+0.32± 1.72	-99.00	LARC
MLO	surface-flask	NOAA	United States	19°32'N, 155°35'W, 3397 masl	1235	0	+1000.00	+0.11	+0.12± 0.61	+0.08± 0.67	+0.17± 0.59	-99.00	MLO
SUM	surface-flask	NOAA	Greenland	72°36'N, 38°25'W, 3209 masl	27	27	+0.75	+0.21	+0.22± 0.58	+0.26± 0.39	+0.15± 0.65	+0.79	SUM
HPB	surface-flask	NOAA	Germany	47°48'N, 11° 1'E, 936 masl	483	458	+5.00	+4.47	+0.67± 3.97	+0.94± 4.01	+0.39± 3.91	+0.64	HPB
CRZ	surface-flask	NOAA	France	46°26'S, 51°51'E, 197 masl	30	30	+0.50	+0.20	+0.03± 0.34	+0.12± 0.28	-0.05± 0.40	+0.54	CRZ
OTA	surface-flask	CSIRO	Australia	38°31'S, 142°49'E, 40 masl	139	0	+1000.00	+0.30	-1.38±19.85	-1.60±13.07	+2.46±17.63	-99.00	OTA
KAS	surface-insitu	AGH	Poland	49°14'N, 19°59'E, 1989 masl	90147	0	+1000.00	+1.59	-0.25± 4.86	+1.76± 4.99	-1.71± 4.24	-99.00	KAS
GCI01	tower-insitu	PSU	United States	32°28'N, 92°17'W, 65 masl	7150	0	+1000.00	+14.82	-1.56±14.97	-1.40±18.79	-1.75±13.41	-99.00	GCI01
ABT	surface-insitu	EC	Canada	49° 2'N, 122°22'W, 100 masl	14758	0	+1000.00	+15.30	-6.29±18.75	-10.08±17.96	-2.83±17.89	-99.00	ABT
ARCPAC2008	aircraft-insitu	NOAA-CSD	United States	Variable	22588	0	+1000.00	+0.94	-0.01± 8.52	+nan± nan	-0.01± 8.52	-99.00	ARCPAC2008
RGL	tower-insitu	UNIVBRIS	United Kingdom	51°60'N, 2°32'W, 204 masl	32072	0	+1000.00	+3.44	-1.68± 5.47	-2.23± 6.39	-0.97± 4.55	-99.00	RGL
DSI	surface-flask	NOAA	Taiwan	20°42'N, 116°44'E, 3 masl	244	0	+1000.00	+0.61	+1.75± 3.20	+2.05± 1.76	+1.83± 3.42	-99.00	DSI
Site code	**Sampling Type**	**Lab.**	**Country**	**Lat, Lon, Elev. (m ASL)**	**No. Obs. Available**	**No. Obs. Assimilated**	**√R (μmol mol^{-1})**	**√HPH (μmol mol^{-1})**	**H(x)-y (μmol mol^{-1})**	**H(x)-y (JJAS) (μmol mol^{-1})**	**H(x)-y (NDJFMA) (μmol mol^{-1})**	**Inn. X^2**	**Site code**
AMT	surface-pfp	NOAA	United States	45° 2'N, 68°41'W, 53 masl	133	0	+1000.00	+4.53	+0.29± 2.18	+0.68± 2.72	+0.08± 1.66	-99.00	AMT
SYO	surface-insitu	TU	Japan	69° 1'S, 39°35'E, 14 masl	6150	0	+1000.00	+0.11	-0.00± 0.25	+0.18± 0.22	-0.12± 0.19	-99.00	SYO
RPB	surface-flask	NOAA	Barbados	13°10'N, 59°26'W, 15 masl	817	791	+1.50	+0.28	-0.04± 0.69	+0.40± 0.66	-0.23± 0.57	+0.22	RPB
MSH	surface-pfp	NOAA	United States	41°39'N, 70°30'W, 32 masl	105	0	+1000.00	+3.25	+1.15± 4.04	+3.41± 4.96	+0.26± 2.87	-99.00	MSH
BRW	surface-flask	NOAA	United States	71°19'N, 156°37'W, 11 masl	52	0	+1000.00	+1.05	+0.05± 0.94	+0.37± 0.98	-0.27± 0.94	-99.00	BRW
FPK	surface-insitu	PSU	United States	48°18'N, 105° 6'W, 634 masl	7733	0	+1000.00	+5.03	-2.47± 9.62	-8.01±18.57	-0.89± 5.33	-99.00	FPK
SCT	tower-insitu	NOAA	United States	33°24'N, 81°50'W, 115 masl	9349	1440	+6.00	+5.51	+0.35± 3.26	+0.47± 3.24	+0.27± 3.22	+0.45	SCT
EEC	surface-insitu	ICTA-UAB	Spain	36° 4'N, 5°40'W, 20 masl	15602	0	+1000.00	+1.46	-1.90± 6.93	-1.86± 6.26	-1.60± 7.03	-99.00	EEC
CRV	aircraft-pfp	NOAA	United States	64°59'N, 147°36'W, 611 masl	2041	0	+1000.00	+2.81	-2.00±10.31	-1.34± 7.55	-0.22± 4.91	-99.00	CRV
POC	shipboard-flask	NOAA	N/A	Variable	2521	2467	+0.87	+0.27	-0.07± 0.64	+0.09± 0.62	-0.16± 0.62	+0.78	POC
OXK	surface-flask	NOAA	Germany	50° 2'N, 11°49'E, 1022 masl	31	31	+5.00	+1.87	-1.76± 4.34	-1.18± 5.38	-2.44± 2.85	+0.78	OXK
CIB	surface-flask	NOAA	Spain	41°49'N, 4°56'W, 845 masl	345	317	+2.51	+3.35	+0.38± 2.20	+0.21± 2.25	+0.40± 2.04	+0.74	CIB
RTA	aircraft-pfp	NOAA	Cook Islands	21°15'S, 159°50'W, 3 masl	2442	0	+1000.00	+0.12	-0.12± 0.67	+0.15± 0.51	-0.32± 0.72	-99.00	RTA
RGV	surface-insitu	PSU	United States	44° 5'N, 91°20'W, 251 masl	18137	0	+1000.00	+11.00	-1.11± 9.99	-1.61±13.58	-0.30± 5.11	-99.00	RGV
LJO	surface-flask	SIO	United States	32°52'N, 117°15'W, 10 masl	339	333	+5.02	+0.83	+4.22± 2.65	+5.94± 2.75	+3.25± 2.11	+1.06	LJO
Site code	**Sampling Type**	**Lab.**	**Country**	**Lat, Lon, Elev. (m ASL)**	**No. Obs. Available**	**No. Obs. Assimilated**	**√R (μmol mol^{-1})**	**√HPH (μmol mol^{-1})**	**H(x)-y (μmol mol^{-1})**	**H(x)-y (JJAS) (μmol mol^{-1})**	**H(x)-y (NDJFMA) (μmol mol^{-1})**	**Inn. X^2**	**Site code**

HBA	surface-flask	NOAA	United Kingdom	75°36'S, 26°13'W, 30 masl	3	3	+0.50	+0.25	-0.38± 0.13	+nan± nan	-0.38± 0.13	+1.05	HBA
AZR	surface-flask	NOAA	Portugal	38°46'N, 27°23'W, 19 masl	482	461	+1.50	+0.47	+0.26± 1.25	+0.36± 1.45	+0.32± 1.19	+0.75	AZR
WSA	surface-insitu	EC	Canada	43°56'N, 60° 1'W, 5 masl	1153	232	+5.59	+2.35	+0.06± 1.17	+nan± nan	+0.45± 1.02	+0.08	WSA
GCI05	tower-insitu	PSU	United States	30°12'N, 85°50'W, 5 masl	14834	0	+1000.00	+13.50	-2.26±11.95	-2.94±13.49	-1.10± 9.98	-99.00	GCI05
UTUOU	tower-insitu	U-ATAQ	United States	40°46'N, 111°51'W, 1427 masl	115523	0	+1000.00	+4.27	-10.75±19.53	-5.00± 9.24	-15.89±24.58	-99.00	UTUOU
SEY	surface-flask	NOAA	Seychelles	4°41'S, 55°32'E, 2 masl	30	30	+0.75	+0.19	+0.35± 1.25	+0.36± 0.39	+0.35± 1.85	+3.20	SEY
HSU	surface-flask	NOAA	United States	41° 4'N, 124°45'W, 0 masl	4	0	+1000.00	+17.59	-1.47± 2.44	+nan± nan	-2.31± 1.97	-99.00	HSU
CES	tower-insitu	ECN	the Netherlands	51°58'N, 4°56'E, -1 masl	109512	0	+1000.00	+6.39	-1.74±10.85	-1.43±11.00	-1.78±10.95	-99.00	CES
WBI	surface-pfp	NOAA	United States	41°43'N, 91°21'W, 241 masl	168	0	+1000.00	+6.81	-1.15± 3.38	-1.48± 4.16	-1.07± 2.80	-99.00	WBI
OSI	tower-insitu	OSU	United States	44°60'N, 122°42'W, 351 masl	28990	0	+1000.00	+6.37	+0.40± 7.48	-1.07± 8.24	+1.56± 5.86	-99.00	OSI
WBI	aircraft-pfp	NOAA	United States	41°43'N, 91°21'W, 241 masl	98	0	+1000.00	+1.06	+0.10± 0.86	-0.16± 0.46	+0.16± 0.87	-99.00	WBI
SEY	surface-flask	NOAA	Seychelles	4°41'S, 55°32'E, 2 masl	739	718	+0.75	+0.18	-0.12± 0.73	+0.07± 0.51	-0.33± 0.83	+1.00	SEY
HUN	tower-insitu	HMS	Hungary	46°57'N, 16°39'E, 248 masl	127379	20705	+5.98	+10.04	-0.11± 3.43	+0.38± 3.25	-0.37± 3.49	+0.60	HUN
LLN	surface-flask	NOAA	Taiwan	23°28'N, 120°52'E, 2862 masl	388	0	+1000.00	+0.29	+1.73± 5.95	+1.27± 9.05	+1.81± 3.42	-99.00	LLN
LUT	surface-insitu	RUG	Netherlands	53°24'N, 6°21'E, 1 masl	68732	0	+1000.00	+6.66	-4.10± 9.46	-5.27±11.28	-3.11± 7.82	-99.00	LUT
Site code	**Sampling Type**	**Lab.**	**Country**	**Lat, Lon, Elev. (m ASL)**	**No. Obs. Available**	**No. Obs. Assimilated**	**√R (μmol mol^{-1})**	**√HPH (μmol mol^{-1})**	**H(x)-y (μmol mol^{-1})**	**H(x)-y (JJAS) (μmol mol^{-1})**	**H(x)-y (NDJFMA) (μmol mol^{-1})**	**Inn. χ^2**	**Site code**
LARC	aircraft-insitu	NASA-LaRC	United States	Variable	28069	0	+1000.00	+0.11	+0.75± 0.78	+0.75± 0.78	+nan± nan	-99.00	LARC
DSI	surface-flask	NOAA	Taiwan	20°42'N, 116°44'E, 3 masl	41	0	+1000.00	+0.39	+2.96± 2.93	+2.58± 2.46	+3.71± 3.01	-99.00	DSI
BRM	tower-insitu	KUP	Switzerland	47°11'N, 8°11'E, 797 masl	33402	0	+1000.00	+8.28	+1.06±10.71	-0.33±11.49	+1.98±10.19	-99.00	BRM
MLO	surface-flask	CSIRO	United States	19°32'N, 155°35'W, 3397 masl	546	0	+1000.00	+0.10	+0.19± 0.66	+0.02± 0.60	+0.35± 0.69	-99.00	MLO
CYA	surface-flask	CSIRO	Australia	66°17'S, 110°31'E, 47 masl	381	381	+0.57	+0.10	-0.00± 0.28	+0.18± 0.25	-0.11± 0.26	+0.30	CYA
BSC	surface-flask	NOAA	Romania	44°11'N, 28°40'E, 0 masl	458	0	+1000.00	+3.92	-8.27±13.35	-13.87±16.17	-4.32± 7.73	-99.00	BSC
HBA	surface-flask	NOAA	United Kingdom	75°36'S, 26°13'W, 30 masl	750	740	+0.50	+0.14	+0.12± 0.26	+0.31± 0.25	+0.00± 0.20	+0.38	HBA
HNP	surface-insitu	EC	Canada	43°37'N, 79°23'W, 87 masl	17086	0	+1000.00	+13.03	-3.57±15.01	-6.13±18.75	-0.80± 9.76	-99.00	HNP
FTL	aircraft-pfp	NOAA	Brazil	3°31'S, 38°17'W, 3 masl	160	0	+1000.00	+0.25	-0.44± 1.39	+0.20± 1.43	-0.97± 0.91	-99.00	FTL
POC	shipboard-flask	NOAA	N/A	Variable	88	88	+0.79	+0.14	-0.08± 0.70	+0.04± 0.41	-0.18± 0.83	+0.94	POC
MCI	aircraft-pfp	NOAA	United States	Variable	128	0	+1000.00	+6.10	+0.18± 4.40	+0.36± 5.80	+0.56± 2.67	-99.00	MCI
TAC	tower-insitu	UNIVBRIS	United Kingdom	52°31'N, 1° 8'E, 56 masl	27849	0	+1000.00	+3.91	-0.67± 5.98	-1.04± 7.04	-0.34± 5.27	-99.00	TAC
SCT	surface-pfp	NOAA	United States	33°24'N, 81°50'W, 115 masl	1753	0	+1000.00	+4.10	-0.38± 3.67	-0.08± 3.75	-0.70± 3.73	-99.00	SCT
RCE	surface-insitu	PSU	United States	40°48'N, 92°53'W, 286 masl	15256	0	+1000.00	+12.40	+1.08±11.85	+1.01±14.94	+2.58± 6.81	-99.00	RCE
TIK	surface-flask	NOAA	Russia	71°36'N, 128°53'E, 19 masl	42	0	+1000.00	+4.87	-0.73± 7.76	-5.46± 7.64	+1.02± 2.61	-99.00	TIK
Site code	**Sampling Type**	**Lab.**	**Country**	**Lat, Lon, Elev. (m ASL)**	**No. Obs. Available**	**No. Obs. Assimilated**	**√R (μmol mol^{-1})**	**√HPH (μmol mol^{-1})**	**H(x)-y (μmol mol^{-1})**	**H(x)-y (JJAS) (μmol mol^{-1})**	**H(x)-y (NDJFMA) (μmol mol^{-1})**	**Inn. χ^2**	**Site code**
SMO	surface-flask	NOAA	American Samoa	14°15'S, 170°34'W, 42 masl	75	0	+1000.00	+0.11	-0.19± 0.69	+0.35± 0.21	-0.68± 0.66	-99.00	SMO
RTA	aircraft-pfp	NOAA	Cook Islands	21°15'S, 159°50'W, 3 masl	35	0	+1000.00	+0.12	-0.58± 0.43	+nan± nan	-0.58± 0.43	-99.00	RTA
ACV	surface-insitu	PSU	United States	39° 7'N, 79°27'W, 1026 masl	22824	0	+1000.00	+6.24	-5.99±12.98	-11.91±18.21	-1.79± 5.21	-99.00	ACV
INX	aircraft-pfp	NOAA	United States	Variable	332	0	+1000.00	+5.08	-0.03± 4.68	+1.18± 6.80	-0.81± 3.40	-99.00	INX
BHD	surface-flask	NOAA	New Zealand	41°24'S, 174°52'E, 85 masl	225	213	+0.75	+0.23	+0.15± 0.70	+0.52± 0.67	-0.08± 0.61	+1.00	BHD
LARC	aircraft-insitu	NASA-LaRC	United States	Variable	52938	0	+1000.00	+2.90	+0.74± 3.93	+0.74± 3.93	+nan± nan	-99.00	LARC
MRC	surface-pfp	NOAA	United States	41°42'N, 76° 0'W, -9999999999999999455752309870428160 masl	181	0	+1000.00	+7.06	-0.93± 5.96	-1.12± 7.93	-1.09± 3.40	-99.00	MRC
OLI	surface-insitu	LBNL-ARM	United States	70°30'N, 149°53'W, 2 masl	775955	0	+1005.94	+2.51	-1.45± 4.20	-1.63± 5.08	-1.30± 3.26	-99.00	OLI
CIT	surface-insitu	CALTECH	United States	34° 8'N, 118° 8'W, 233 masl	31410	0	+1000.00	+3.33	-15.46±26.04	-7.93±16.50	-22.86±31.52	-99.00	CIT
BKT	surface-flask	NOAA	Indonesia	0°12'S, 100°19'E, 845 masl	27	0	+1000.00	+0.61	+6.56± 3.43	+8.01± 3.89	+5.38± 2.78	-99.00	BKT
SMR	tower-insitu	UHELS	Finland	61°51'N, 24°18'E, 181 masl	31189	0	+1000.00	+3.67	-0.14± 4.50	-0.62± 5.92	+0.45± 3.54	-99.00	SMR
RRL	surface-insitu	PSU	United States	43°32'N, 95°25'W, 469 masl	18565	0	+1000.00	+8.51	+0.73± 7.88	+0.83±11.06	+1.20± 4.04	-99.00	RRL
GMI	surface-flask	NOAA	Guam	13°23'N, 144°39'E, 0 masl	22	22	+0.75	+0.09	+0.43± 0.93	-0.19± 0.48	+0.48± 0.94	+1.89	GMI
STR	surface-pfp	NOAA	United States	37°45'N, 122°27'W, 254 masl	4563	3946	+4.02	+2.00	-0.24± 2.34	-0.03± 2.28	-0.32± 2.40	+0.37	STR
CES	tower-insitu	ECN	the Netherlands	51°58'N, 4°56'E, -1 masl	109693	0	+1000.00	+3.83	-2.09± 7.97	-1.30± 7.79	-2.66± 8.27	-99.00	CES

Site code	Sampling Type	Lab.	Country	Lat, Lon, Elev. (m ASL)	No. Obs. Available	No. Obs. Assimilated	$\sqrt{R}$ (μmol mol^{-1})	$\sqrt{HPH}$ (μmol mol^{-1})	H(x)-y (μmol mol^{-1})	H(x)-y (JJAS) (μmol mol^{-1})	H(x)-y (NDJFMA) (μmol mol^{-1})	Inn. X^2	Site code
LLB	surface-insitu	EC	Canada	54°57'N, 112°27'W, 540 masl	1910	327	+5.52	+4.31	-0.49± 2.68	+nan± nan	-0.49± 2.72	+0.45	LLB
ACT	aircraft-insitu	NASA-LaRC	United States	Variable	144181	0	+1000.55	+2.26	+0.24± 2.33	+nan± nan	+0.34± 2.00	-99.00	ACT
LIN	surface-insitu	HPB	Germany	52° 7'N, 14° 7'E, 73 masl	7843	0	+1000.00	+5.84	-0.42± 9.09	-2.51±10.60	+1.77± 7.49	-99.00	LIN
ESP	aircraft-pfp	NOAA	Canada	49°23'N, 126°33'W, 7 masl	209	0	+1000.00	+4.03	-0.45± 4.84	-0.27± 6.19	-0.37± 0.89	-99.00	ESP
THD	aircraft-pfp	NOAA	United States	41° 3'N, 124° 9'W, 107 masl	118	0	+1000.00	+1.38	+0.04± 3.59	-0.29± 4.11	+0.33± 3.83	-99.00	THD
NOR	tower-insitu	LUND-CEC	Sweden	60° 5'N, 17°29'E, 45 masl	16765	0	+1000.00	+3.50	-3.22± 8.12	-6.02±11.58	-1.37± 4.44	-99.00	NOR
SYO	surface-flask	NOAA	Japan	69° 1'S, 39°35'E, 14 masl	398	395	+0.50	+0.11	+0.03± 0.27	+0.24± 0.24	-0.11± 0.21	+0.35	SYO
PSA	surface-flask	SIO	United States	64°55'S, 64° 0'W, 10 masl	391	0	+1000.00	+0.28	+0.19± 0.31	+0.34± 0.27	+0.10± 0.31	-99.00	PSA
TPD	surface-insitu	EC	Canada	42°37'N, 80°33'W, 231 masl	35392	0	+1000.00	+14.92	-1.74±15.06	-7.06±21.74	+2.03± 7.96	-99.00	TPD
CIB	surface-flask	NOAA	Spain	41°49'N, 4°56'W, 845 masl	38	34	+2.50	+3.18	+0.40± 2.04	-0.23± 1.96	+0.81± 1.91	+0.51	CIB
INX	surface-pfp	NOAA	United States	Variable	1717	0	+1000.00	+8.36	-0.50± 7.99	-0.39±10.44	-1.07± 6.55	-99.00	INX
TAC	tower-insitu	UNIVBRIS	United Kingdom	52°31'N, 1° 8'E, 56 masl	23302	0	+1000.00	+2.90	-0.58± 4.71	-0.70± 5.66	-0.42± 4.08	-99.00	TAC
ZEP	surface-flask	NOAA	Norway and Sweden	78°54'N, 11°53'E, 474 masl	46	45	+1.50	+0.57	+0.33± 0.88	+0.35± 1.11	+0.21± 0.76	+0.50	ZEP
BCS	surface-flask	SIO_CO2	Mexico	23°18'N, 110°12'W, 4 masl	172	0	+1000.00	+0.78	-1.12± 3.87	-2.93± 4.91	+0.54± 1.95	-99.00	BCS
PFA	aircraft-pfp	NOAA	United States	65° 4'N, 147°17'W, 210 masl	4018	0	+1000.00	+1.09	+0.11± 1.80	+0.39± 2.40	+0.10± 1.40	-99.00	PFA
Site code	Sampling Type	Lab.	Country	Lat, Lon, Elev. (m ASL)	No. Obs. Available	No. Obs. Assimilated	$\sqrt{R}$ (μmol mol^{-1})	$\sqrt{HPH}$ (μmol mol^{-1})	H(x)-y (μmol mol^{-1})	H(x)-y (JJAS) (μmol mol^{-1})	H(x)-y (NDJFMA) (μmol mol^{-1})	Inn. X^2	Site code
INX04	surface-insitu	PSU	United States	39°36'N, 86° 7'W, 249 masl	3336	0	+1000.00	+12.83	-2.81±13.07	-4.80±18.15	-1.74±10.71	-99.00	INX04
LARC	aircraft-insitu	NASA-LaRC	United States	Variable	30057	0	+1000.00	+2.40	-1.69± 6.25	-1.69± 6.25	+nan± nan	-99.00	LARC
GCI02	tower-insitu	PSU	United States	33°45'N, 89°51'W, 105 masl	10667	0	+1000.00	+12.63	-0.67±13.64	+0.89±16.47	-1.87±10.80	-99.00	GCI02
NAT	surface-flask	NOAA	Brazil	5°48'S, 35°11'W, 50 masl	235	229	+1.50	+0.16	-0.63± 0.97	-0.43± 1.01	-0.84± 0.94	+0.62	NAT
TPD	surface-insitu	EC	Canada	42°37'N, 80°33'W, 231 masl	3441	0	+1000.00	+13.20	+1.34±12.25	+nan± nan	+2.57±11.53	-99.00	TPD
LARC	aircraft-insitu	NASA-LaRC	United States	Variable	57339	0	+1000.00	+1.38	+0.39± 4.05	+0.18± 5.22	+0.67± 1.45	-99.00	LARC
BRA	surface-insitu	EC	Canada	51°12'N, 104°42'W, 595 masl	3354	583	+5.40	+6.13	+0.06± 1.85	+nan± nan	+0.05± 1.84	+0.21	BRA
ACT	aircraft-pfp	NOAA	United States	Variable	118	0	+1000.00	+5.30	-0.84± 4.79	-0.84± 4.79	+nan± nan	-99.00	ACT
NAT	surface-flask	IPEN	Brazil	5°48'S, 35°11'W, 50 masl	201	0	+1000.00	+0.16	-0.57± 1.09	-0.43± 1.31	-0.68± 0.95	-99.00	NAT
TOM	aircraft-insitu	NOAA	United States	Variable	32054	0	+1000.00	+0.26	+0.13± 1.16	+nan± nan	+0.13± 1.16	-99.00	TOM
SPO	surface-insitu	NOAA	United States	89°59'S, 24°48'W, 2810 masl	9010	1386	+0.98	+0.10	-0.03± 0.27	+0.29± 0.12	-0.23± 0.16	+0.11	SPO
PAL	surface-insitu	FMI	Finland	67°58'N, 24° 7'E, 565 masl	28523	0	+1000.00	+2.94	-0.48± 3.53	-0.37± 4.59	-0.27± 3.01	-99.00	PAL
ASC	surface-flask	NOAA	United Kingdom	7°58'S, 14°24'W, 85 masl	60	60	+0.75	+0.19	+0.48± 0.90	+0.99± 0.52	+0.11± 1.03	+1.90	ASC
LJO	surface-flask	SIO_CO2	United States	32°52'N, 117°15'W, 10 masl	425	0	+1000.00	+1.34	+8.21± 7.63	+11.46± 7.01	+6.07± 6.65	-99.00	LJO
KEY	surface-flask	NOAA	United States	25°40'N, 80° 9'W, 1 masl	32	31	+1.50	+0.48	+0.01± 0.74	+0.03± 0.58	-0.09± 0.81	+0.18	KEY
Site code	Sampling Type	Lab.	Country	Lat, Lon, Elev. (m ASL)	No. Obs. Available	No. Obs. Assimilated	$\sqrt{R}$ (μmol mol^{-1})	$\sqrt{HPH}$ (μmol mol^{-1})	H(x)-y (μmol mol^{-1})	H(x)-y (JJAS) (μmol mol^{-1})	H(x)-y (NDJFMA) (μmol mol^{-1})	Inn. X^2	Site code
KEY	surface-flask	NOAA	United States	25°40'N, 80° 9'W, 1 masl	695	571	+1.50	+1.22	+0.02± 0.89	+0.13± 0.86	-0.05± 0.93	+0.37	KEY
BMW	surface-flask	NOAA	United Kingdom	32°16'N, 64°53'W, 30 masl	32	29	+1.50	+0.58	+1.09± 1.39	+0.89± 1.47	+1.17± 1.06	+1.32	BMW
CBY	surface-insitu	EC	Canada	69° 1'N, 105° 3'W, 35 masl	28815	5660	+5.54	+2.12	+0.07± 1.15	-0.25± 1.53	+0.22± 0.87	+0.07	CBY
MBO	tower-insitu	NOAA	United States	43°59'N, 121°41'W, 2731 masl	4503	0	+1000.00	+1.20	+0.45± 3.03	+0.24± 3.34	+0.70± 2.41	-99.00	MBO
BCK	surface-insitu	EC	Canada	62°48'N, 116° 3'W, 179 masl	3406	683	+5.60	+2.53	+0.41± 1.11	+nan± nan	+0.49± 1.03	+0.07	BCK
WSA	surface-insitu	EC	Canada	43°56'N, 60° 1'W, 5 masl	88924	17286	+5.50	+1.70	+0.10± 1.88	+0.67± 2.47	-0.17± 1.49	+0.17	WSA
UTSUG	tower-insitu	U-ATAQ	United States	40°44'N, 111°51'W, 1328 masl	79469	0	+1000.00	+5.22	-21.24±30.33	-12.13±18.35	-29.32±36.50	-99.00	UTSUG
MHD	surface-insitu	LSCE	Ireland	53°20'N, 9°54'W, 5 masl	35535	0	+1000.00	+0.41	+0.20± 0.94	+0.55± 1.08	+0.02± 0.79	-99.00	MHD
DEC	surface-insitu	ICTA-UAB	Spain	40°45'N, 0°47'E, 5 masl	19482	0	+1000.00	+4.83	-0.88± 9.67	-1.08±11.60	-0.70± 8.04	-99.00	DEC
HEI	surface-insitu	UHEI-IUP	Germany	49°25'N, 8°40'E, 116 masl	123793	0	+1000.00	+7.20	-8.65±14.96	-8.28±14.05	-8.84±15.68	-99.00	HEI
STR	surface-pfp	NOAA	United States	37°45'N, 122°27'W, 254 masl	576	249	+3.00	+2.21	-0.48± 2.62	-0.02± 2.13	-0.84± 2.97	+0.85	STR
LARC	aircraft-insitu	NASA-LaRC	United States	Variable	8004	0	+1000.00	+1.01	+0.02± 1.62	+nan± nan	-0.22± 1.68	-99.00	LARC
DRP	shipboard-flask	NOAA	N/A	59° 0'S, 64°41'W, 0 masl	219	219	+0.51	+0.22	+0.02± 0.34	+0.17± 0.39	-0.06± 0.32	+0.50	DRP
TAP	surface-flask	NOAA	Republic of Korea	36°44'N, 126° 8'E, 16 masl	42	41	+5.40	+2.04	+2.29± 5.53	+2.00± 3.52	+3.77± 5.27	+1.58	TAP

INX12	surface-insitu	PSU	United States	39°46'N, 86° 2'W, 254 masl	2983	0	+1000.00	+13.20	-6.63±14.46	-10.11±20.41	-5.51±12.38	-99.00	INX12
Site code	**Sampling Type**	**Lab.**	**Country**	**Lat, Lon, Elev. (m ASL)**	**No. Obs. Available**	**No. Obs. Assimilated**	**√R (µmol mol^{-1})**	**√HPH (µmol mol^{-1})**	**H(x)-y (µmol mol^{-1})**	**H(x)-y (JJAS) (µmol mol^{-1})**	**H(x)-y (NDJFMA) (µmol mol^{-1})**	**Inn. X^2**	**Site code**
UTA	surface-flask	NOAA	United States	39°54'N, 113°43'W, 1327 masl	770	733	+2.50	+1.60	+0.20± 2.03	+0.65± 2.25	-0.28± 1.69	+0.67	UTA
ENA	surface-insitu	LBNL-ARM	Portugal	39° 5'N, 28° 2'W, 30 masl	611997	0	+1001.11	+0.52	-1.15± 3.87	-1.54± 5.03	-0.80± 3.43	-99.00	ENA
INX10	surface-insitu	PSU	United States	39°43'N, 86° 9'W, 223 masl	5136	0	+1000.00	+14.76	-6.80±15.76	-8.21±18.42	-5.42±12.51	-99.00	INX10
WGC	tower-insitu	NOAA	United States	38°16'N, 121°29'W, 0 masl	9269	1395	+6.00	+5.05	+0.04± 3.53	+0.76± 2.83	-0.23± 3.92	+0.64	WGC
ELL	surface-flask	ICTA-UAB	Spain	42°34'N, 0°57'E, 2002 masl	139	0	+1000.00	+0.87	+0.95± 1.89	+1.68± 1.80	+0.02± 1.51	-99.00	ELL
LARC	aircraft-insitu	NASA-LaRC	United States	Variable	56390	0	+1000.00	+2.12	-0.10± 3.19	-0.10± 3.19	+nan± nan	-99.00	LARC
CALNEX2010	aircraft-insitu	NOAA-CSD	United States	Variable	39373	0	+1000.00	+3.54	-0.66±14.05	-0.43±12.34	+1.10± 7.76	-99.00	CALNEX2010
ALT	surface-flask	SIO	Canada	82°27'N, 62°30'W, 190 masl	384	0	+1000.00	+0.48	+0.26± 0.69	+0.12± 0.76	+0.36± 0.69	-99.00	ALT
AAC	surface-insitu	PSU	United States	29°44'N, 82°13'W, 44 masl	2145	0	+1000.00	+9.50	-0.74± 9.14	+1.16± 9.53	-0.71± 9.26	-99.00	AAC
BAO	tower-insitu	NOAA	United States	40° 3'N, 105° 0'W, 1584 masl	70854	11271	+9.83	+5.03	-1.49± 3.60	-0.96± 3.14	-2.12± 3.88	+0.18	BAO
OIL	aircraft-pfp	NOAA	United States	41°17'N, 88°56'W, 192 masl	424	0	+1000.00	+2.14	+0.59± 2.26	+0.62± 3.03	+0.45± 1.25	-99.00	OIL
YON	surface-insitu	JMA	Japan	24°28'N, 123° 1'E, 30 masl	82580	0	+1000.00	+0.39	+0.08± 1.77	+0.32± 1.63	+0.18± 1.76	-99.00	YON
AIA	aircraft-flask	CSIRO	Australia	40°32'S, 144°18'E, 0 masl	63	0	+1000.00	+0.15	+0.33± 0.55	+0.33± 0.55	+nan± nan	-99.00	AIA
MWO	surface-pfp	NOAA	United States	34°13'N, 118° 4'W, 1728 masl	2283	0	+1000.00	+0.55	-2.30± 5.11	-2.46± 5.37	-2.05± 4.95	-99.00	MWO
COP	tower-insitu	HU	United States	42°21'N, 71° 5'W, 6 masl	35850	0	+1000.00	+8.24	-2.75±13.09	-2.60±17.18	-3.14±10.02	-99.00	COP
Site code	**Sampling Type**	**Lab.**	**Country**	**Lat, Lon, Elev. (m ASL)**	**No. Obs. Available**	**No. Obs. Assimilated**	**√R (µmol mol^{-1})**	**√HPH (µmol mol^{-1})**	**H(x)-y (µmol mol^{-1})**	**H(x)-y (JJAS) (µmol mol^{-1})**	**H(x)-y (NDJFMA) (µmol mol^{-1})**	**Inn. X^2**	**Site code**
BME	surface-flask	NOAA	United Kingdom	32°22'N, 64°39'W, 12 masl	244	231	+1.50	+0.64	+0.52± 1.24	+1.13± 1.21	+0.21± 1.23	+0.93	BME
LEF	aircraft-pfp	NOAA	United States	45°57'N, 90°16'W, 472 masl	3431	0	+1000.00	+2.80	-0.02± 2.50	+0.18± 3.57	-0.02± 1.49	-99.00	LEF
MNM	surface-insitu	JMA	Japan	24°17'N, 153°59'E, 8 masl	109810	0	+1000.00	+0.21	+0.29± 0.77	+0.24± 0.80	+0.44± 0.74	-99.00	MNM
CBA	surface-flask	SIO	United States	55°13'N, 162°43'W, 21 masl	350	0	+1000.00	+0.52	-0.04± 1.96	+0.79± 2.90	-0.39± 0.94	-99.00	CBA
FNE	surface-insitu	EC	Canada	58°50'N, 122°34'W, 361 masl	10455	0	+1000.00	+7.88	-12.12±19.49	-15.24±23.50	-9.38±13.84	-99.00	FNE
ESP	surface-insitu	EC	Canada	49°23'N, 126°33'W, 7 masl	3036	546	+5.45	+2.19	-0.12± 1.62	+nan± nan	-0.15± 1.61	+0.11	ESP
SDZ	surface-flask	NOAA	Peoples Republic of China	40°39'N, 117° 7'E, 293 masl	257	0	+1000.00	+3.36	-2.15± 8.68	-3.24±10.81	-1.14± 6.95	-99.00	SDZ
RK1	surface-flask	SIO_CO2	Raoul Island	29°12'S, 177°54'W, 2 masl	115	0	+1000.00	+0.30	-0.61± 2.36	+0.05± 0.57	-0.90± 1.01	-99.00	RK1
TGC	aircraft-pfp	NOAA	United States	27°44'N, 96°52'W, 0 masl	86	0	+1000.00	+0.66	+0.64± 0.97	+0.53± 1.01	+0.77± 1.08	-99.00	TGC
ASC	surface-flask	NOAA	United Kingdom	7°58'S, 14°24'W, 85 masl	1466	1444	+0.75	+0.19	-0.07± 0.75	+0.33± 0.63	-0.40± 0.71	+1.12	ASC
WBI	aircraft-pfp	NOAA	United States	41°43'N, 91°21'W, 241 masl	1959	0	+1000.00	+2.72	+0.05± 2.67	-0.13± 3.02	+0.35± 1.56	-99.00	WBI
LMU	surface-insitu	ICTA-UAB	Spain	41°36'N, 1° 6'W, 571 masl	6143	0	+1000.00	+3.73	-0.89± 6.20	-0.50± 5.35	-0.60± 5.11	-99.00	LMU
ICE	surface-flask	NOAA	Iceland	63°24'N, 20°17'W, 118 masl	30	30	+1.50	+0.49	+0.34± 1.27	+1.06± 1.54	-0.05± 1.11	+0.75	ICE
THD	surface-flask	NOAA	United States	41° 3'N, 124° 9'W, 107 masl	675	646	+5.08	+2.52	-1.84± 3.51	-2.17± 3.87	-1.42± 3.02	+0.62	THD
OMT	surface-insitu	OSU	United States	44°27'N, 121°33'W, 1255 masl	79073	0	+1000.00	+2.79	-0.41± 4.72	-1.30± 5.76	+0.23± 3.71	-99.00	OMT
Site code	**Sampling Type**	**Lab.**	**Country**	**Lat, Lon, Elev. (m ASL)**	**No. Obs. Available**	**No. Obs. Assimilated**	**√R (µmol mol^{-1})**	**√HPH (µmol mol^{-1})**	**H(x)-y (µmol mol^{-1})**	**H(x)-y (JJAS) (µmol mol^{-1})**	**H(x)-y (NDJFMA) (µmol mol^{-1})**	**Inn. X^2**	**Site code**
MWO	surface-pfp	NOAA	United States	34°13'N, 118° 4'W, 1728 masl	466	0	+1000.00	+0.71	-2.53± 5.37	-2.98± 5.11	-2.11± 5.44	-99.00	MWO
AMY	surface-flask	NOAA	Republic of Korea	36°32'N, 126°20'E, 85 masl	126	0	+1000.00	+2.87	-3.17± 9.97	-5.25±10.47	-1.16± 9.15	-99.00	AMY
SPO	surface-flask	SIO	United States	89°59'S, 24°48'W, 2810 masl	396	0	+1000.00	+0.09	+0.17± 0.30	+0.44± 0.22	-0.00± 0.23	-99.00	SPO
EGB	surface-insitu	EC	Canada	44°14'N, 79°47'W, 251 masl	90404	8950	+4.87	+9.78	+0.05± 2.35	+0.51± 2.78	-0.12± 2.19	+0.44	EGB
BRM	tower-insitu	KUP	Switzerland	47°11'N, 8°11'E, 797 masl	33398	0	+1000.00	+8.64	+0.55±11.15	-0.82±11.87	+1.44±10.66	-99.00	BRM
WLG	surface-flask	NOAA	Peoples Republic of China	36°17'N, 100°54'E, 3810 masl	38	35	+1.50	+1.02	-0.05± 1.34	+0.28± 1.55	+0.02± 1.07	+1.08	WLG
WGC	tower-insitu	NOAA	United States	38°16'N, 121°29'W, 0 masl	75428	11663	+5.90	+4.78	+0.33± 3.29	+1.27± 2.74	-0.07± 3.55	+0.48	WGC
NAT	surface-flask	NOAA	Brazil	5°48'S, 35°11'W, 50 masl	37	37	+1.50	+0.17	+0.40± 1.06	+0.94± 0.77	-0.04± 1.19	+0.55	NAT
WIS	surface-flask	NOAA	Israel	29°58'N, 35° 4'E, 151 masl	857	825	+2.50	+0.48	-0.29± 1.98	+0.23± 1.70	-0.45± 1.95	+0.65	WIS
AME	surface-insitu	PSU	United States	41°10'N, 96°28'W, 362 masl	36708	0	+1000.00	+9.85	-8.76±26.95	-21.57±43.18	-1.61± 7.88	-99.00	AME
OXK	surface-flask	NOAA	Germany	50° 2'N, 11°49'E, 1022 masl	410	396	+5.00	+1.74	-0.66± 3.51	-0.31± 3.74	-1.19± 3.45	+0.55	OXK
LMP	surface-flask	NOAA	Italy	35°31'N, 12°37'E, 45 masl	437	415	+1.50	+1.31	+0.28± 1.37	-0.26± 1.36	+0.68± 1.27	+0.90	LMP

LMP	surface-flask	NOAA	Italy	35°31'N, 12°37'E, 45 masl	36	34	+1.50	+1.04	+0.58± 1.33	-0.17± 1.13	+1.27± 1.25	+1.09	LMP
MLO	surface-flask	SIO	United States	19°32'N, 155°35'W, 3397 masl	629	0	+1000.00	+0.10	+0.28± 0.68	+0.19± 0.62	+0.36± 0.75	-99.00	MLO
EIC	surface-flask	NOAA	Chile	27°10'S, 109°26'W, 47 masl	562	529	+1.50	+0.11	+0.27± 1.09	+0.74± 0.90	-0.13± 1.02	+0.58	EIC
Site code	**Sampling Type**	**Lab.**	**Country**	**Lat, Lon, Elev. (m ASL)**	**No. Obs. Available**	**No. Obs. Assimilated**	**$\sqrt{R}$ ($\mu mol\ mol^{-1}$)**	**$\sqrt{HPH}$ ($\mu mol\ mol^{-1}$)**	**H(x)-y ($\mu mol\ mol^{-1}$)**	**H(x)-y (JJAS) ($\mu mol\ mol^{-1}$)**	**H(x)-y (NDJFMA) ($\mu mol\ mol^{-1}$)**	**Inn. χ^2**	**Site code**
SPL	surface-insitu	NCAR	United States	40°27'N, 106°44'W, 3210 masl	71929	0	+1000.00	+0.54	-0.47± 1.92	+0.01± 2.36	-0.84± 1.49	-99.00	SPL
BRW	surface-flask	NOAA	United States	71°19'N, 156°37'W, 11 masl	8939	866	+1.38	+1.30	+0.20± 0.72	+0.49± 0.93	+0.09± 0.61	+0.87	BRW
SCA	aircraft-pfp	NOAA	United States	32°46'N, 79°33'W, 0 masl	2791	0	+1000.00	+1.25	+0.23± 1.98	+0.04± 2.57	+0.34± 1.50	-99.00	SCA
CHR	surface-flask	NOAA	Republic of Kiribati	1°42'N, 157° 9'W, 0 masl	536	524	+0.75	+0.15	-0.38± 0.54	-0.24± 0.45	-0.45± 0.57	+0.84	CHR
MEX	surface-flask	NOAA	Mexico	18°59'N, 97°19'W, 4464 masl	307	306	+2.50	+0.40	+0.78± 1.52	+1.37± 1.63	+0.30± 1.09	+0.47	MEX
WIS	surface-flask	NOAA	Israel	29°58'N, 35° 4'E, 151 masl	39	39	+2.50	+0.38	+0.05± 1.39	+0.27± 1.62	-0.16± 1.29	+0.30	WIS
GMI	surface-flask	NOAA	Guam	13°23'N, 144°39'E, 0 masl	1024	969	+0.75	+0.09	+0.24± 0.81	+0.22± 0.93	+0.33± 0.71	+1.31	GMI
LLN	surface-flask	NOAA	Taiwan	23°28'N, 120°52'E, 2862 masl	33	0	+1000.00	+0.29	+0.42± 1.86	+0.83± 1.80	+0.63± 1.62	-99.00	LLN
BRW	surface-flask	SIO_CO2	United States	71°19'N, 156°37'W, 11 masl	800	0	+1000.00	+2.41	-1.31±35.69	+0.02± 4.18	-2.95±50.61	-99.00	BRW
HDP	surface-insitu	NCAR	United States	40°34'N, 111°39'W, 3351 masl	62719	0	+1000.00	+0.38	-0.16± 1.39	-0.17± 1.72	-0.19± 1.13	-99.00	HDP
OBN	surface-flask	NOAA	Russia	55° 7'N, 36°36'E, 183 masl	136	132	+5.03	+3.65	-0.21± 3.68	-1.67± 3.73	+0.67± 3.51	+0.61	OBN
MHD	surface-flask	NOAA	Ireland	53°20'N, 9°54'W, 5 masl	744	667	+1.50	+1.39	+0.10± 0.94	+0.31± 1.07	+0.01± 0.85	+0.43	MHD
FIK	surface-flask	LSCE	Greece	35°20'N, 25°40'E, 150 masl	241	0	+1000.00	+1.11	+0.45± 2.88	+0.38± 3.53	+0.65± 2.67	-99.00	FIK
GCI03	tower-insitu	PSU	United States	31°53'N, 89°44'W, 132 masl	10856	0	+1000.00	+13.38	-2.73±15.57	-2.61±19.19	-3.71±10.84	-99.00	GCI03
WPC	shipboard-flask	NOAA	N/A	Variable	265	0	+1000.00	+0.22	-0.08± 1.12	+0.20± 0.76	-0.10± 1.39	-99.00	WPC
Site code	**Sampling Type**	**Lab.**	**Country**	**Lat, Lon, Elev. (m ASL)**	**No. Obs. Available**	**No. Obs. Assimilated**	**$\sqrt{R}$ ($\mu mol\ mol^{-1}$)**	**$\sqrt{HPH}$ ($\mu mol\ mol^{-1}$)**	**H(x)-y ($\mu mol\ mol^{-1}$)**	**H(x)-y (JJAS) ($\mu mol\ mol^{-1}$)**	**H(x)-y (NDJFMA) ($\mu mol\ mol^{-1}$)**	**Inn. χ^2**	**Site code**
CES	tower-insitu	ECN	the Netherlands	51°58'N, 4°56'E, -1 masl	107970	0	+1000.00	+6.61	-5.42±14.60	-7.06±16.40	-4.16±12.81	-99.00	CES
SPO	surface-flask	CSIRO	United States	89°59'S, 24°48'W, 2810 masl	166	0	+1000.00	+0.09	-0.03± 0.32	+0.16± 0.31	-0.19± 0.27	-99.00	SPO
THD	aircraft-pfp	NOAA	United States	41° 3'N, 124° 9'W, 107 masl	1975	0	+1000.00	+1.99	+0.14± 2.59	-0.19± 2.83	+0.42± 2.58	-99.00	THD
INX01	surface-insitu	PSU	United States	39°35'N, 86°25'W, 256 masl	10364	0	+1000.00	+12.14	+0.71±11.80	-0.03±15.12	+0.43± 6.89	-99.00	INX01
HTM	tower-insitu	LUND-CEC	Sweden	56° 6'N, 13°25'E, 115 masl	6787	0	+1000.00	+3.94	-1.77± 5.89	-2.00± 7.54	-1.65± 4.52	-99.00	HTM
LARC	aircraft-insitu	NASA-LaRC	United States	Variable	37889	0	+1000.00	+2.19	-0.58± 2.01	-0.79± 1.88	+nan± nan	-99.00	LARC
HSU	surface-flask	NOAA	United States	41° 4'N, 124°45'W, 0 masl	78	0	+1000.00	+7.99	+2.36± 9.30	+0.06± 2.53	+4.71±12.98	-99.00	HSU
MSH	surface-pfp	NOAA	United States	41°39'N, 70°30'W, 32 masl	65	0	+1000.00	+3.44	+0.48± 5.01	+0.56± 6.19	-0.84± 2.25	-99.00	MSH
CBA	surface-flask	NOAA	United States	55°13'N, 162°43'W, 21 masl	1245	1119	+1.51	+0.52	-0.51± 1.47	+0.46± 1.73	-0.99± 1.01	+1.19	CBA
LEF	surface-pfp	NOAA	United States	45°57'N, 90°16'W, 472 masl	2743	0	+1000.00	+4.64	-0.10± 3.34	+0.48± 4.69	-0.27± 2.24	-99.00	LEF
HUN	surface-flask	NOAA	Hungary	46°57'N, 16°39'E, 248 masl	821	0	+1000.00	+7.43	-0.64± 4.95	+0.26± 4.37	-0.85± 5.42	-99.00	HUN
CGO	surface-flask	NOAA	Australia	40°41'S, 144°41'E, 94 masl	38	38	+0.50	+0.24	+0.06± 0.86	+0.57± 0.52	-0.46± 0.99	+3.24	CGO
NOR	tower-insitu	LUND-CEC	Sweden	60° 5'N, 17°29'E, 45 masl	16768	0	+1000.00	+3.39	-2.32± 6.70	-4.34± 9.45	-1.04± 4.10	-99.00	NOR
EST	surface-insitu	EC	Canada	51°40'N, 110°12'W, 707 masl	56090	7373	+5.29	+5.63	-0.20± 2.15	-0.09± 2.86	-0.23± 1.98	+0.30	EST
MBO	tower-insitu	NOAA	United States	43°59'N, 121°41'W, 2731 masl	22195	0	+1000.00	+0.97	-0.12± 3.66	-0.81± 4.71	+0.17± 1.98	-99.00	MBO
Site code	**Sampling Type**	**Lab.**	**Country**	**Lat, Lon, Elev. (m ASL)**	**No. Obs. Available**	**No. Obs. Assimilated**	**$\sqrt{R}$ ($\mu mol\ mol^{-1}$)**	**$\sqrt{HPH}$ ($\mu mol\ mol^{-1}$)**	**H(x)-y ($\mu mol\ mol^{-1}$)**	**H(x)-y (JJAS) ($\mu mol\ mol^{-1}$)**	**H(x)-y (NDJFMA) ($\mu mol\ mol^{-1}$)**	**Inn. χ^2**	**Site code**
OWA	surface-insitu	OSU	United States	44° 4'N, 123°38'W, 715 masl	31316	0	+1000.00	+2.80	-1.18± 4.17	-1.49± 5.00	-0.60± 3.40	-99.00	OWA
CRV	tower-insitu	NOAA	United States	64°59'N, 147°36'W, 611 masl	38268	0	+1000.00	+2.32	+0.26± 6.30	+0.02±10.00	+0.76± 2.51	-99.00	CRV
RPB	surface-flask	NOAA	Barbados	13°10'N, 59°26'W, 15 masl	47	47	+1.50	+0.26	+0.21± 0.58	+0.71± 0.53	-0.13± 0.37	+0.18	RPB
ULB	aircraft-pfp	NOAA	Mongolia	47°24'N, 106° 0'E, 1350 masl	517	517	+2.00	+0.71	+0.20± 1.18	+0.27± 1.40	+0.22± 1.15	+0.69	ULB
CFA	surface-flask	CSIRO	Australia	19°17'S, 147° 3'E, 2 masl	334	331	+1.63	+0.57	-0.48± 1.05	-0.21± 1.25	-0.72± 0.88	+0.52	CFA
BRW	surface-flask	NOAA	United States	71°19'N, 156°37'W, 11 masl	1012	0	+1000.00	+1.36	-0.10± 1.49	+0.04± 2.02	-0.16± 1.08	-99.00	BRW
BRA	surface-insitu	EC	Canada	51°12'N, 104°42'W, 595 masl	46629	6770	+5.38	+6.86	-0.09± 2.03	-0.51± 2.84	-0.01± 1.83	+0.27	BRA
CPS	surface-insitu	EC	Canada	49°49'N, 74°59'W, 381 masl	41211	6458	+5.31	+4.47	+0.12± 1.96	+0.66± 2.60	-0.02± 1.58	+0.23	CPS
SAN	aircraft-pfp	NOAA	Brazil	2°51'S, 54°57'W, 78 masl	322	309	+2.00	+0.58	+0.10± 1.81	-0.26± 1.70	+0.46± 1.99	+1.07	SAN
GAT	surface-insitu	HPB	Germany	53° 4'N, 11°27'E, 70 masl	5037	0	+1000.00	+3.20	-1.69± 6.24	-1.09± 5.54	-3.34± 6.04	-99.00	GAT
ARA	surface-flask	CSIRO	Australia	23°52'S, 148°28'E, 175 masl	22	0	+1000.00	+1.44	-1.34± 2.55	-0.89± 1.79	-1.14± 0.89	-99.00	ARA

NHA	aircraft-pfp	NOAA	United States	42°57'N, 70°38'W, 0 masl	3285	0	+1000.00	+1.84	+0.27± 2.38	+0.43± 3.37	+0.26± 1.75	-99.00	NHA
AMS	surface-insitu	LSCE	France	37°48'S, 77°32'E, 55 masl	126809	0	+1000.00	+0.20	-0.25± 0.86	+0.26± 0.52	-0.73± 0.87	-99.00	AMS
ORC	aircraft-insitu	NCAR	Chile	Variable	40217	0	+1000.00	+0.24	-0.78± 1.04	+nan± nan	-0.78± 1.04	-99.00	ORC
MRC	surface-pfp	NOAA	United States	41°28'N, 76°25'W, 651 masl	135	0	+1000.00	+7.37	-0.58± 7.90	+0.78±11.55	-1.51± 5.37	-99.00	MRC
Site code	**Sampling Type**	**Lab.**	**Country**	**Lat, Lon, Elev. (m ASL)**	**No. Obs. Available**	**No. Obs. Assimilated**	**$\sqrt{R}$ (μmol mol^{-1})**	**$\sqrt{HPH}$ (μmol mol^{-1})**	**H(x)-y (μmol mol^{-1})**	**H(x)-y (JJAS) (μmol mol^{-1})**	**H(x)-y (NDJFMA) (μmol mol^{-1})**	**Inn. X^2**	**Site code**
CPT	surface-insitu	SAWS	South Africa	34°21'S, 18°29'E, 230 masl	113029	0	+1000.00	+0.30	+0.10± 0.82	+0.65± 0.73	-0.28± 0.66	-99.00	CPT
GIC	surface-insitu	ICTA-UAB	Spain	40°21'N, 5°11'W, 1436 masl	25820	0	+1000.00	+1.34	-8.64±15.97	-15.36±21.12	-4.96±10.78	-99.00	GIC
UUM	surface-flask	NOAA	Mongolia	44°27'N, 111° 6'E, 1007 masl	801	751	+2.50	+1.08	-0.15± 2.48	-0.69± 2.85	+0.34± 2.11	+1.03	UUM
CGO	surface-flask	CSIRO	Australia	40°41'S, 144°41'E, 94 masl	837	0	+1000.00	+0.12	+0.13± 0.36	+0.40± 0.28	-0.10± 0.29	-99.00	CGO
JFJ	surface-insitu	KUP	Switzerland	46°33'N, 7°59'E, 3570 masl	87610	14539	+2.97	+0.79	+0.05± 1.60	+0.17± 1.45	-0.05± 1.74	+0.34	JFJ
XIC	surface-insitu	ICTA-UAB	Spain	41°59'N, 8° 1'W, 890 masl	5553	0	+1000.00	+1.33	-0.78± 3.85	-0.02± 3.91	-0.62± 3.76	-99.00	XIC
SGP	surface-flask	NOAA	United States	36°36'N, 97°29'W, 314 masl	685	645	+3.00	+4.66	-0.27± 2.26	-0.63± 2.63	+0.02± 1.89	+0.59	SGP
CBA	surface-flask	NOAA	United States	55°13'N, 162°43'W, 21 masl	83	78	+1.50	+0.58	-0.66± 1.29	-0.83± 1.52	-0.43± 1.08	+0.99	CBA
TIK	surface-flask	NOAA	Russia	71°36'N, 128°53'E, 19 masl	251	0	+1000.00	+5.85	+0.03± 7.80	-3.77± 6.15	+2.21± 8.56	-99.00	TIK
RBA-B	aircraft-pfp	IPEN	Brazil	9°22'S, 67°36'W, -9999999999999999455752309870428160 masl	675	0	+1000.00	+1.22	-0.05± 3.60	+0.73± 4.14	-0.02± 3.08	-99.00	RBA-B
CHL	surface-insitu	EC	Canada	58°45'N, 94° 4'W, 29 masl	28854	5522	+5.55	+4.17	+0.16± 1.56	-0.05± 2.18	+0.27± 1.08	+0.11	CHL
FSD	surface-insitu	EC	Canada	49°53'N, 81°34'W, 210 masl	3297	620	+5.51	+5.96	+0.12± 1.70	+nan± nan	+0.20± 1.69	+0.14	FSD
PTA	surface-flask	NOAA	United States	38°57'N, 123°44'W, 17 masl	428	395	+5.01	+3.34	-2.27± 3.56	-1.61± 3.56	-2.48± 3.53	+0.69	PTA
HPB	surface-flask	NOAA	Germany	47°48'N, 11° 1'E, 936 masl	39	37	+5.00	+4.53	+1.82± 3.84	+2.33± 4.51	+1.15± 2.93	+0.56	HPB
TAC	tower-insitu	UNIVBRIS	United Kingdom	52°31'N, 1° 8'E, 56 masl	27798	0	+1000.00	+4.07	-1.84± 7.01	-2.79± 8.54	-1.15± 5.88	-99.00	TAC
Site code	**Sampling Type**	**Lab.**	**Country**	**Lat, Lon, Elev. (m ASL)**	**No. Obs. Available**	**No. Obs. Assimilated**	**$\sqrt{R}$ (μmol mol^{-1})**	**$\sqrt{HPH}$ (μmol mol^{-1})**	**H(x)-y (μmol mol^{-1})**	**H(x)-y (JJAS) (μmol mol^{-1})**	**H(x)-y (NDJFMA) (μmol mol^{-1})**	**Inn. X^2**	**Site code**
CRV	surface-pfp	NOAA	United States	64°59'N, 147°36'W, 611 masl	881	0	+1000.00	+2.17	+0.55± 3.31	+1.06± 4.44	+0.49± 2.17	-99.00	CRV
ABP	surface-flask	IPEN	Brazil	12°46'S, 38°10'W, 1 masl	104	0	+1000.00	+0.42	-1.04± 1.43	-0.53± 1.36	-1.54± 1.30	-99.00	ABP
FSD	surface-insitu	EC	Canada	49°53'N, 81°34'W, 210 masl	129507	19416	+5.23	+6.46	-0.05± 2.06	+0.19± 2.81	-0.06± 1.67	+0.30	FSD
OFR	surface-insitu	OSU	United States	44°39'N, 123°33'W, 263 masl	58193	0	+1000.00	+7.82	-0.09± 9.53	-0.20±10.96	+0.37± 8.47	-99.00	OFR
SHM	surface-flask	NOAA	United States	52°43'N, 174° 8'E, 23 masl	54	53	+2.50	+0.64	-0.11± 1.74	+0.93± 2.10	-0.56± 0.94	+0.60	SHM
PAL	surface-insitu	FMI	Finland	67°58'N, 24° 7'E, 565 masl	23687	23687	+9.49	+1.45	-0.04± 1.20	+0.23± 1.65	-0.10± 0.97	+0.03	PAL
ESP	aircraft-pfp	NOAA	Canada	49°23'N, 126°33'W, 7 masl	3800	0	+1000.00	+2.87	+0.04± 2.90	-0.09± 4.07	+0.15± 1.88	-99.00	ESP
MLO	surface-flask	SIO_CO2	United States	19°32'N, 155°35'W, 3397 masl	877	0	+1000.00	+0.11	+0.22± 0.67	+0.16± 0.71	+0.31± 0.66	-99.00	MLO
AMT	tower-insitu	NOAA	United States	45° 2'N, 68°41'W, 53 masl	9382	1441	+6.00	+7.76	+0.23± 2.51	+0.78± 3.05	+0.04± 2.17	+0.23	AMT
PRS	surface-insitu	RSE	Italy	45°56'N, 7°42'E, 3480 masl	61520	0	+1000.00	+0.82	+0.13± 1.66	+0.80± 1.85	-0.18± 1.54	-99.00	PRS
AZR	surface-flask	NOAA	Portugal	38°46'N, 27°23'W, 19 masl	5	5	+1.50	+0.63	+0.40± 0.30	+nan± nan	+0.40± 0.30	+0.07	AZR
NWR	surface-pfp	NOAA	United States	40° 3'N, 105°35'W, 3523 masl	2320	0	+1000.00	+0.58	+0.61± 1.94	+1.51± 2.42	+0.04± 1.34	-99.00	NWR
CRV	aircraft-pfp	NOAA	United States	64°59'N, 147°36'W, 611 masl	344	0	+1000.00	+2.70	+0.76± 3.41	+0.78± 3.63	+0.34± 0.94	-99.00	CRV
RMM	surface-insitu	PSU	United States	41° 8'N, 96°27'W, 358 masl	16623	0	+1000.00	+8.60	+0.16± 8.57	-1.13±11.75	+1.62± 4.62	-99.00	RMM
BHD	surface-insitu	NIWA	New Zealand	41°24'S, 174°52'E, 85 masl	537	537	+0.78	+0.20	+0.27± 0.53	+0.47± 0.49	+0.08± 0.53	+0.69	BHD
Site code	**Sampling Type**	**Lab.**	**Country**	**Lat, Lon, Elev. (m ASL)**	**No. Obs. Available**	**No. Obs. Assimilated**	**$\sqrt{R}$ (μmol mol^{-1})**	**$\sqrt{HPH}$ (μmol mol^{-1})**	**H(x)-y (μmol mol^{-1})**	**H(x)-y (JJAS) (μmol mol^{-1})**	**H(x)-y (NDJFMA) (μmol mol^{-1})**	**Inn. X^2**	**Site code**
PSA	surface-flask	NOAA	United States	64°55'S, 64° 0'W, 10 masl	24	24	+0.50	+0.26	+0.03± 0.27	+0.19± 0.24	+0.01± 0.23	+0.40	PSA
ETL	surface-insitu	EC	Canada	54°21'N, 104°59'W, 492 masl	3404	662	+5.54	+5.65	+0.19± 1.46	+nan± nan	+0.27± 1.33	+0.12	ETL
MLO	surface-insitu	NOAA	United States	19°32'N, 155°35'W, 3397 masl	8970	992	+1.40	+0.11	+0.35± 0.61	+0.17± 0.48	+0.39± 0.67	+0.32	MLO
HIL	aircraft-pfp	NOAA	United States	40° 4'N, 87°55'W, 201 masl	107	0	+1000.00	+1.60	-0.03± 1.44	+0.95± 1.42	-0.10± 1.40	-99.00	HIL
MID	surface-flask	NOAA	United States	28°13'N, 177°23'W, 11 masl	41	40	+1.50	+0.24	+0.93± 1.26	+1.14± 1.62	+0.86± 0.96	+1.28	MID
INX	surface-pfp	NOAA	United States	39°35'N, 86°25'W, 256 masl	237	0	+1000.00	+8.16	-1.63± 6.52	-4.25±10.32	-0.93± 3.10	-99.00	INX
UTA	surface-flask	NOAA	United States	39°54'N, 113°43'W, 1327 masl	46	44	+2.50	+0.54	-0.06± 2.21	-0.38± 2.22	-0.33± 2.10	+0.87	UTA
SHM	surface-flask	NOAA	United States	52°43'N, 174° 8'E, 23 masl	650	591	+2.50	+0.52	-0.06± 1.95	+1.46± 2.22	-0.98± 1.06	+0.73	SHM
CMA	aircraft-pfp	NOAA	United States	38°50'N, 74°19'W, 0 masl	2429	0	+1000.00	+2.04	+0.17± 2.49	-0.10± 3.34	+0.36± 1.75	-99.00	CMA
HUN	surface-flask	NOAA	Hungary	46°57'N, 16°39'E, 248 masl	32	0	+1000.00	+8.49	-0.93± 8.33	+2.56± 6.32	-6.37± 7.66	-99.00	HUN

3. Further Reading

- **ESRL Carbon Cycle Program**
- **WMO/GAW Report No. 206, 2012**
- **ICOS**

Ensemble Data Assimilation [go to top]

1. Introduction

Data assimilation is the name of a process by which observations of the 'state' of a system help to constrain the behavior of the system in time. An example of one of the earliest applications of data assimilation is the system in which the trajectory of a flying rocket is constantly (and rapidly) adjusted based on information of its current position to guide it to its exact final destination. Another example of data assimilation is a weather model that gets updated every few hours with measurements of temperature and other variables, to improve the accuracy of its forecast for the next day, and the next, and the next. Data assimilation is usually a cyclical process, as estimates get refined over time as more observations about the "truth" become available. Mathematically, data assimilation can be done with any number of techniques. For large systems, so-called variational and ensemble techniques have gained most popularity. Because of the size and complexity of the systems studied in most fields, data assimilation projects inevitably include supercomputers that model the known physics of a system. Success in guiding these models in time often depends strongly on the number of observations available to inform on the true system state.

In CarbonTracker, the model that describes the system contains relatively simple descriptions of biospheric and oceanic CO_2 exchange, as well as fossil fuel and fire emissions. In time, we alter the behavior of this model by adjusting a set of parameters as described in the next section.

2. Detailed Description

The four surface flux modules drive instantaneous CO_2 fluxes in CarbonTracker according to:

$F(x, y, t) = \lambda(x,y,t) \cdot F_{bio}(x, y, t) + \lambda(x,y,t) \cdot F_{oce}(x, y, t) + F_{ff}(x, y, t) + F_{fire}(x, y, t)$

Where λ represents a set of linear scaling factors applied to the fluxes, to be estimated in the assimilation. These scaling factors are the final product of our assimilation and together with the modules determine the fluxes we present in CarbonTracker. Note that no scaling factors are applied to the fossil fuel and fire modules.

2.1 Land-surface classification

The scaling factors λ are estimated for each week and assumed constant over this period. Each scaling factor is associated with a particular gridbox of the global domain. We chose an approach in which the ocean grid boxes are combined into 30 large basins encompassing large-scale ocean circulation features, as in the TransCom inversion study (e.g. Gurney et al., [2002]). The terrestrial biosphere grid boxes are combined up according to ecosystem type as well as geographical location. Thereto, each of the 11 TransCom land regions contains a maximum of 19 ecosystem types summarized in the table below for Europe.

Ecosystem types considered on 1x1 degree for the terrestrial flux inversions is based on **Olson, [1992]**. Note that we have adjusted the original 29 categories into only 19 regions. This was done mainly to fill the unused categories 16,17, and 18, and to group the similar (from our perspective) categories 23-26+29. The table below shows each vegetation category considered. Percentages indicate the area associated with each category for Europe rounded to one decimal.

Ecosystem Types and area in Europe

category	Olson V 1.3a	%
1	Conifer Forest	14.0
2	Broadleaf Forest	2.5
3	Mixed Forest	8.9
4	Grass/Shrub	8.0
5	Tropical Forest	0.1
6	Scrub/Woods	2.8
7	Semitundra	4.9
8	Fields/Woods/Savanna	6.6
9	Northern Taiga	2.2
10	Forest/Field	11.5
11	Wetland	0.7
12	Deserts	0.1
13	Shrub/Tree/Suc	0.0
14	Crops	22.3
15	Conifer Snowy/Coastal	0.0
16	Wooded tundra	1.6
17	Mangrove	0.0
18	Ice and Polar desert	0.0
19	Water	13.8
99	All	100.0

Each 1x1 degree pixel of our domain was assigned one of the categories above bases on the Olson category that was most prevalent in the 0.5x0.5 degree underlying area.

2.2 Ensemble Size and Localization

The ensemble system used to solve for the scalar multiplication factors is similar to that in Peters et al. [2005] and based on the square root ensemble Kalman filter of Whitaker and Hamill, [2002]. We have restricted the length of the smoother window to only five weeks as we found the derived flux patterns within Europe and North America to be robustly resolved well within that time. We caution the CarbonTracker users that although the North American and European flux results were found to be robust after five weeks, regions of the world with less dense observational coverage (the tropics, Southern Hemisphere, and parts of Asia) are likely to be poorly observable even after more than a month of transport and therefore less robustly resolved. Although longer assimilation windows, or long prior covariance length-scales, could potentially help to constrain larger scale emission totals from such areas, we focus our analysis here on a region more directly constrained by real atmospheric observations.

Ensemble statistics are created from 150 ensemble members, each with its own background CO_2 concentration field to represent the time history (and thus covariances) of the filter. In contrast to our earlier system design, we currently do not apply any localization to the statevector.

2.3 Dynamical Model

In CarbonTracker, the dynamical model is applied to the mean parameter values λ as:

$\lambda_t^b = (\lambda_{t-2}^a + \lambda_{t-1}^a + \lambda^p) / 3.0$

Where "a" refers to analyzed quantities from previous steps, "b" refers to the background values for the new step, and "p" refers to real *a-priori* determined values that are fixed in time and chosen as part of the inversion set-up. Physically, this model describes that parameter values λ for a new time step are chosen as a combination between optimized values from the two previous time steps, and a fixed prior value. This operation is similar to the simple persistence forecast used in Peters et al. [2005], but represents a smoothing over three time steps thus dampening variations in the forecast of λ^b in time. The inclusion of the prior term λ^p acts as a regularization [Baker et al., 2006] and ensures that the parameters in our system will eventually revert back to predetermined prior values when there is no information coming from the observations. Note that our dynamical model equation does not include an error term on the dynamical model, for the simple reason that we don't know the error of this model. This is reflected in the treatment of covariance, which is always set to a prior covariance structure and not forecast with our dynamical model.

2.4 Covariance Structure

Prior values for λ^p are all 1.0 to yield fluxes that are unchanged from their values predicted in our modules. The prior covariance structure P^p describes the magnitude of the uncertainty on each parameter, plus their correlation in space.

In each of these regions on the northern hemisphere, individual λ(x,y) parameters are coupled through an isentropic covariance structure which makes two boxes i and j at a distance d of each other have a covariance C of

$C = 0.64 \cdot \exp(-d/L)$.

In this formula the covariance length scale L varies across the globe. Over Boral and Temperate North America where the observation network is relatively dense, L=300km, but in Boreal and Temperate Asia the number of observations constrains a much smaller number of parameters individually and we chose L=1000km. In Europe, with its strongly heterogeneous land-use and land management and large volume of observations available we took L=200km. In the rest of the world, the length scale is taken infiniely large, coupling fully all grid boxes and associated λ's in the tropics and southern hemisphere.

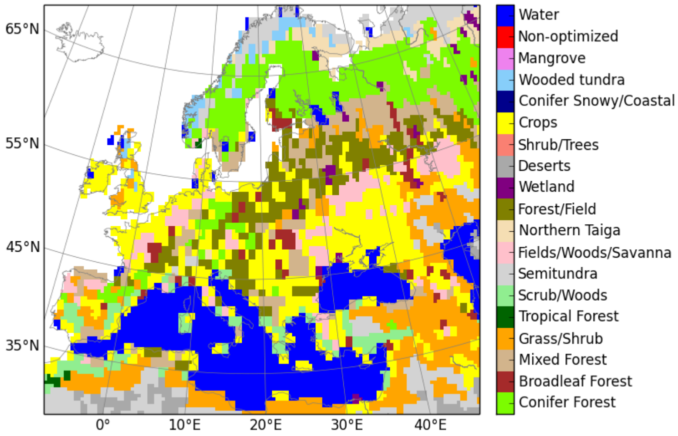

The figure shows ecoregions for Europe (**click here for global land ecoregions**). Note that there is currently no requirement for ecoregions to be contiguous, and a single scaling factor can be applied to the same vegetation type on both sides of a continent.

Theoretically, this approach leads to a total number of 9835 optimizable scaling factors λ each week, but the actual number is smaller since not every ecosystem type is represented in each **TransCom region**, and because we decided not to optimize parameters for ice-covered regions, inland water bodies, and desert. The total flux coming out of these last regions is negligibly small. It is important to note that even though many parameters are available to scale the fluxes, the imposed covariance structure reduces the number of degrees of freedom to about 1100 each week.

Furthermore, all ecosystems *within* tropical **TransCom regions** are coupled decreasing exponentially with distance since we do not believe the current observing network can constrain tropical fluxes on sub-continental scales, and want to prevent large dipoles to occur in the tropics.

In our standard assimilation, the chosen standard deviation is 80% on land parameters, and 40% on ocean parameters. This reflects more prior confidence in the ocean fluxes than in terrestrial fluxes, as is assumed often in inversion studies and partly reflects the lower variability and larger homogeneity of the ocean fluxes. All parameters have the same variance within the land or ocean domain. Because the parameters multiply the net-flux though, ecosystems with larger weekly mean net fluxes have a larger variance in absolute flux magnitude.

3. Further Reading

- **Whitaker and Hamill, 2002 paper**
- **Peters et al., 2005 paper**
- **Olson ecosystem types, data**